Archival Report

Biological Psychiatry

Dynamic Resting-State Network Biomarkers of Antidepressant Treatment Response

Roselinde H. Kaiser, Henry W. Chase, Mary L. Phillips, Thilo Deckersbach, Ramin V. Parsey, Maurizio Fava, Patrick J. McGrath, Myrna Weissman, Maria A. Oquendo, Melvin G. McInnis, Thomas Carmody, Crystal M. Cooper, Madhukar H. Trivedi, and Diego A. Pizzagalli

ABSTRACT

BACKGROUND: Delivery of effective antidepressant treatment has been hampered by a lack of objective tools for predicting or monitoring treatment response. This study aimed to address this gap by testing novel dynamic resting-state functional network markers of antidepressant response.

METHODS: The Establishing Moderators and Biosignatures of Antidepressant Response in Clinical Care (EMBARC) study randomized adults with major depressive disorder to 8 weeks of either sertraline or placebo, and depression severity was evaluated longitudinally. Participants completed resting-state neuroimaging pretreatment and again after 1 week of treatment (n = 259 eligible for analyses). Coactivation pattern analyses identified recurrent whole-brain states of spatial coactivation, and computed time spent in each state for each participant was the main dynamic measure. Multilevel modeling estimated the associations between pretreatment network dynamics and sertraline response and between early (pretreatment to 1 week) changes in network dynamics and sertraline response.

RESULTS: Dynamic network markers of early sertraline response included increased time in network states consistent with canonical default and salience networks, together with decreased time in network states characterized by coactivation of cingulate and ventral limbic or temporal regions. The effect of sertraline on depression recovery was mediated by these dynamic network changes. In contrast, early changes in dynamic functioning of corticolimbic and frontoinsular-default networks were related to patterns of symptom recovery common across treatment groups.

CONCLUSIONS: Dynamic resting-state markers of early antidepressant response or general recovery may assist development of clinical tools for monitoring and predicting effective intervention.

https://doi.org/10.1016/j.biopsych.2022.03.020

Major depressive disorder (MDD) affects between 18% and 50% of individuals over the life span (1,2) and is associated with high levels of distress, impairment (3), and mortality (4). Progress in treatment development has yielded antidepressant medications that are widely used, tolerable for most patients, and highly effective for a subset of patients (5). However, up to 2 out of 3 patients receiving first-line antidepressant medications do not respond adequately (6), and there are serious consequences and costs of poorly treated depression (7). Accordingly, it is critical to understand who will respond to antidepressant medication and what are the mechanisms of early treatment response to plan and monitor effective intervention.

The clinical import of predicting treatment responsiveness has, in part, motivated precision medicine approaches to identify objective markers that predict who will benefit from a given antidepressant treatment (8). In recent years, empirical investigation into such markers has surged, with special interest in resting-state functional brain network markers that predict or track with treatment response. Resting-state network functioning, e.g., the spatial organization, magnitude, and timing of synchronized activity across distributed brain regions, holds information relevant to individual differences in cognition, emotional processing, and mental health (9). In MDD, abnormalities have been observed in several resting-state networks including the canonical default network (DN), comprising midline and temporal regions involved in introspection and autobiographical thinking; the salience (or ventral attention) network (SN), including insula, midcingulate, and temporoparietal regions engaged in salience-directed attention; the frontoparietal network, including lateral prefrontal and posterior parietal regions recruited during goal-directed attention; and corticolimbic networks and sensorimotor regions involved in affective and sensory processing (10). Building on this evidence, research has suggested that individual differences in the magnitude of such abnormalities may predict antidepressant treatment response, although the nature and direction of such prediction is mixed (11,12). For example, stronger positive pretreatment functional connectivity among areas of the DN has predicted both stronger and weaker response to selective serotonin reuptake inhibitor (SSRI) intervention (11,13), which may depend on the DN

SEE COMMENTARY ON PAGE 526

© 2022 Society of Biological Psychiatry.

ISSN: 0006-3223

Downloaded for Anonymous User (n/a) at Harvard University from ClinicalKey.com by Elsevier on September 15, 2022. For personal use only. No other uses without permission. Copyright ©2022. Elsevier Inc. All rights reserved.

subnetwork (14) or the method for operationalizing resting-state network function. Other research has highlighted dysfunctional connectivity between the insula and areas of the SN or DN, but the specific circuits implicated and direction of effects are inconsistent (15,16). Together, although resting-state biomarkers may hold promise for predicting antidepressant response, findings remain mixed.

There are other gaps in our understanding of treatment-related resting-state biomarkers. First, there are few studies that investigate both neural moderators of treatment response (i.e., pretreatment resting-state markers of response) and mediators of treatment response (i.e., resting-state network changes that correspond with or precede improved mental health) [related review in (11,12)]. While the former can provide probability estimates for who will respond to an antidepressant intervention, the latter is needed to understand mechanisms and efficacy of treatment. For example, prior work has shown that SSRIs have effects on several timescales (17), including fast (within 3–10 days) effects on resting-state functional connectivity (18), and SSRI response in the first week of treatment can predict long-term treatment outcome (19). Therefore, gaining a better understanding of early biomarker mediators of treatment efficacy has translational implications.

A second gap in treatment biomarker research is incorporation of new methods for examining dynamic functioning of resting-state networks. Prior work in this field has focused on static network markers, e.g., abnormalities in networks defined by estimates of the overall correlation in activity among brain regions over extended periods of time. While this approach has value, it cannot capture dynamic patterns of functional coordination as transient networks form, persist, and dissolve, or transitions among networks. Such dynamic patterns are especially important for understanding MDD, a condition characterized by abnormalities in temporal characteristics of thinking and emotional experiences (e.g., intrusive rumination over time) (20). Dynamic properties of resting-state networks are reliable (21), and abnormalities in network dynamics involving areas of the DN and SN have been associated with depression (22,23). Some of the most promising dynamic methods adopt data-driven approaches to identify transient functional networks, which may help to clarify mixed biomarker research in which static activity in the same regions is sometimes related to better, and sometimes to worse, treatment outcome.

This study aimed to address these gaps in the context of the Establishing Moderators and Biosignatures of Antidepressant Response in Clinical Care (EMBARC) study. The EMBARC study recruited a large sample of medication-free patients with MDD and randomly assigned participants to either antidepressant medication (sertraline) or placebo for a period of 8 weeks [phase 1; at 8 weeks, patients entered phase 2 (24)]. Participants completed resting-state neuroimaging at baseline (pretreatment) and 1 week after initiating treatment and were repeatedly evaluated for depression severity over the 8-week trial. Response to treatment was assessed using multilevel mixed effects modeling. Network markers of interest were dynamic measures of time spent in transient functional resting network states at baseline and the change in time-in-states from baseline to 1 week after initiating treatment. Analyses tested pretreatment network dynamics that corresponded with pretreatment symptom severity or predicted recovery and early changes in network dynamics that predicted and mediated sertraline-related recovery. We predicted that dynamic activity of transient networks that overlap with canonical DN and SN would predict symptom change and that changes in the dynamic activity of such networks would mediate sertraline response. Analyses took a data-driven approach to identify transient networks and evaluate associations between network dynamics and treatment outcomes.

METHODS AND MATERIALS

Participants

Participants were 309 adults with MDD recruited to the EMBARC study at Columbia University (New York, NY), Massachusetts General Hospital (Boston, MA), the University of Texas Southwestern Medical Center (Dallas, TX), and the University of Michigan (Ann Arbor, MI). Of this sample, $n = 259$ completed clinical evaluations and resting-state neuroimaging and passed initial motion thresholds (Table 1; Figure S1). The institutional review boards at each site approved the research protocol, and participants provided written informed consent. [See (25) for detailed clinical trial design.]

Procedures

Participants were randomized to receive either sertraline or placebo for a period of 8 weeks (phase 1). Participants received no other form of intervention during the study period. The dosage was titrated using a measurement-based care approach, i.e., dosage was increased based on tolerability and response with a maximum daily dose of 200 mg sertraline or four capsules placebo. Participants completed resting-state functional magnetic resonance imaging at baseline and 1 week after initiating treatment. The Hamilton Depression Rating Scale (HAMD) (26) was administered at baseline, weekly for weeks 1 to 4, and biweekly for weeks 4 to 8. At 8 weeks, participants who were nonresponsive in phase 1 were crossed over for phase 2 (placebo nonresponders assigned to sertraline; sertraline nonresponders assigned to bupropion).

Measures

Hamilton Depression Rating Scale. The 17-item HAMD is a widely used, clinician-administered interview measure of depression severity. Each item of the HAMD was scored on a range of 0 (absent) to 4 (severe), and total (summed) score at each time point provided a measure of depression severity. The following percentages of participants in this analysis completed HAMD measurements: baseline, 100%; week 1, 89%; week 2, 82%; week 3, 81%; week 4, 84%; week 6, 81%; week 8, 80%.

Magnetic Resonance Imaging. See Table S1 for imaging acquisition parameters. Protocols for functional scanning were matched across sites. Resting-state functional magnetic resonance imaging data were collected immediately after anatomical scanning.

Analyses

General Image Preprocessing and Motion Corrections. Functional data were preprocessed and motion corrected using

Downloaded for Anonymous User (n/a) at Harvard University from ClinicalKey.com by Elsevier on September 15, 2022. For personal use only. No other uses without permission. Copyright ©2022. Elsevier Inc. All rights reserved.

Table 1. Demographics and Patient Characteristics

Characteristics	Sertraline, *n* = 128	Placebo, *n* = 131
Age, Years	36.52 (13.28)	35.73 (12.34)
HAMD, Baseline	18.52 (4.47)	18.83 (4.35)
HAMD, Week 8	10.32 (6.81)	12.10 (7.82)
Adherence Out of 7 Evaluations	5.86 (1.83)	6.10 (1.64)
Gender		
Female	89 (69.53%)	83 (63.36%)
Male	39 (30.47%)	48 (36.64%)
Race		
African American or Black	27 (21.10%)	20 (15.27%)
Other	19 (14.84%)	21 (16.03%)
White	82 (64.06%)	90 (68.70%)
Ethnicity		
Hispanic	24 (18.75%)	24 (18.32%)
Not Hispanic or Other	104 (81.25%)	107 (81.68%)
Education		
Partial high school or less	5 (3.91%)	4 (3.05%)
High school	18 (14.06%)	17 (12.98%)
Partial college or 2-year degree	40 (30.47%)	41 (31.30%)
College or 4-year degree	32 (25.00%)	38 (29.01%)
Advanced degree	31 (24.22%)	31 (23.66%)
Not reported	2 (1.56%)	0 (0.00%)
Income, Monthly		
$1000 or less	22 (17.19%)	27 (20.61%)
$1000 to $2000	32 (25.00%)	32 (24.43%)
$2000 to $3000	22 (17.19%)	13 (9.92%)
$3000 to $4000	7 (5.47%)	7 (5.34%)
$4000 to $5000	7 (5.47%)	7 (5.34%)
$5000 to $6000	6 (4.69%)	5 (3.82%)
$6000 or higher	5 (3.91%)	17 (12.98%)
Not reported	27 (21.09%)	23 (17.56%)
Site		
Columbia University	37 (28.91%)	41 (31.30%)
Massachusetts General Hospital	23 (17.97%)	23 (17.56%)
University of Michigan	28 (21.87%)	28 (21.37%)
University of Texas Southwestern Medical Center	40 (31.25%)	39 (29.77%)

Values are presented as mean (SD) or *n* (%).
HAMD, Hamilton Rating Scale for Depression.

SPM12 (http://www.fil.ion.ucl.ac.uk/spm/software/spm12/) and Artifact Detection Tools (http://www.nitrc.org/projects/artifact_detect/) (see the Supplement for details). Scans demonstrating high levels of motion or artifacts (>15% of volumes censored) were excluded from subsequent analyses. After these exclusions, *n* = 259 eligible baseline resting-state scan series and *n* = 229 eligible week 1 resting-state scan series were retained.

Resting-State Coactivation Pattern Analysis. Coactivation pattern (CAP) analysis is a data-driven analytic technique that uses the spatial distribution and magnitude of activation at each individual volume and location of whole-brain data as input to a clustering analysis to identify recurring states of relative coactivation across the brain. CAP analyses were performed using MATLAB (version R2019; The MathWorks, Inc.) and the same method we applied in prior work (e.g., in a Human Connectome Project sample; Supplement) (21,23). First, for each participant and each volume, activation (signal relative to the within-participant global mean at that spatial location) was calculated at each of 130 regions of interest in a whole-brain parcellation of the cortex and striatum (27,28) plus subcortical limbic regions as defined by the Automated Anatomical Labeling atlas (details in the Supplement). This step yielded a data vector of coactivation estimates for each volume at each region of interest and for each participant. Second, coactivation data were concatenated across volumes and participants. Third, *k*-means clustering was used to partition the data into *k* brain states that represented recurring patterns of coactivation that emerged over participants and over time. Based on (29) (discussion in the Supplement), *k* values of 5 to 11 were tested, and silhouette scores (a measure of cohesiveness within clusters) were compared across solutions. There were no statistically significant differences in silhouette scores between clustering solutions (*p* values $>$ .20); however, silhouette scores were relatively higher for $k = 7$ or 8 (median silhouette score = 0.111) than other *k* solutions (median silhouette scores = 0.089–0.10). Therefore, and also guided by our prior work indicating 8-cluster solutions in independent samples (21,23), $k = 8$ was selected. Fourth, for each participant and each scan (baseline, 1 week), we computed CAP time-in-state for each network state as the proportion of volumes that the participant spent in that network state during the scan. Changes in network state dynamics were computed by subtracting baseline time-in-state from week 1 time-in-state. This yielded the CAP variables 1) baseline time in each of the CAP states and 2) change in time in each CAP state over the initial week of treatment. All CAP variables were inspected for non-normality or outliers, and any variables that violated assumptions of normal distribution were natural-log transformed (Table S2 and Supplement). Finally, associations among time-in-state measures for CAP network states were tested to identify spatially distinctive states that showed similar dynamic patterns (Table S3). To mitigate potential collinearity when network variables were entered together into multilevel models, network variables that were highly correlated were *z*-scored and averaged to create composite baseline or early-change measures of network dynamics.

Multilevel Mixed Effects Modeling. Mixed effects modeling was performed in R. All models covaried gender and age. A simple model tested linear and nonlinear changes in HAMD scores over the 8-week period, covarying age and gender and including random intercepts and slopes for the associations between time and HAMD scores. To test antidepressant effects, treatment group (sertraline vs. placebo) was contrast-coded and included in the above model as a categorical moderator of the effect of time. Next, two complementary models tested experimental hypotheses. In the first model, testing baseline network dynamics as predictors of treatment response, baseline network dynamics were entered as moderators of the interaction between time and treatment group

Downloaded for Anonymous User (n/a) at Harvard University from ClinicalKey.com by Elsevier on September 15, 2022. For personal use only. No other uses without permission. Copyright ©2022. Elsevier Inc. All rights reserved.

predicting HAMD change. In the second model, testing early network changes as predictors of treatment response, changes in network dynamics were entered as moderators of the relationship between time and HAMD change, controlling for treatment group and baseline network dynamics. Together, a total of three mixed effects models tested hypotheses. For significant paths detected in the latter model, the indirect effect of treatment on HAMD slope through network dynamic change variables were tested (a total of three mediation models were tested). All tests were two-tailed, and the *p* statistics are also reported after false discovery rate (FDR) correction.

RESULTS

Resting-State Networks and Measures of Dynamic Functioning

The eight CAP states are shown in Figure 1 (see also Tables S2–S6 and the Supplement for data quality and

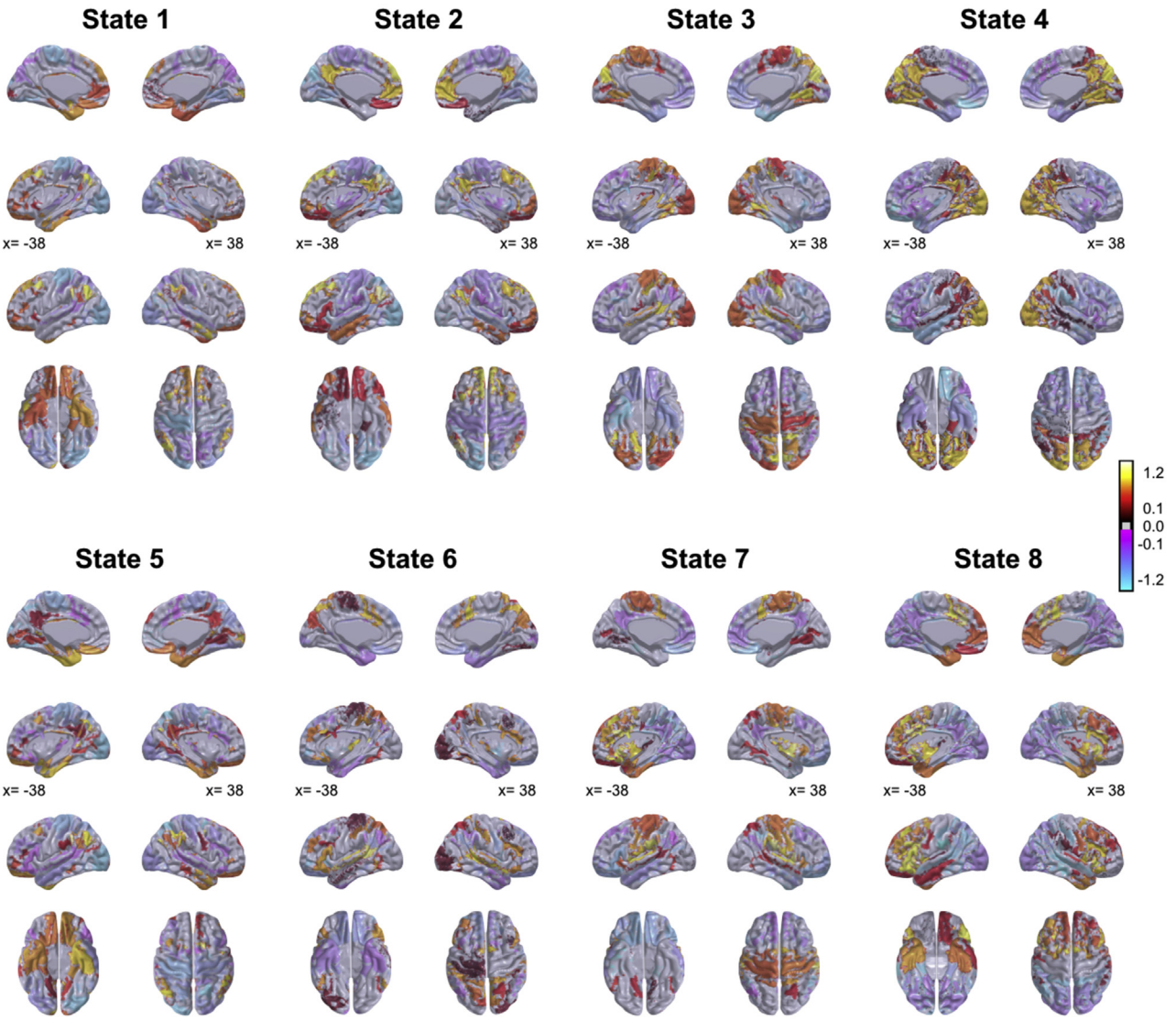

Figure 1. Transient resting-state networks. Coactivation pattern analysis yielded k = 8 resting-state networks that recurred across time, scan series, and participants. State 1 involved corticolimbic regions and overlapped with anterior areas involved in emotion regulation including coactivation of areas of the temporal pole and limbic regions, orbitofrontal cortex, and medial prefrontal cortex. State 2 included regions of the canonical default network and featured midline cortical systems and angular gyrus, as well as middle temporal regions. State 3 was composed of coactivation among sensorimotor regions extending to the parahippocampal cortex. State 4 was characterized by coactivation of occipital regions and posterior parietal regions including the posterior cingulate. State 5 overlapped with posterior areas of the canonical affective and default networks, featuring coactivation of temporal, limbic, orbitofrontal, and posterior cingulate areas. State 6 involved midcingulate and parietal regions, including the posterior dorsal anterior cingulate cortex extending to the supplementary motor area, and superior temporal gyrus. State 7 overlapped with anterior areas of the canonical salience network, including anterior insula, temporoparietal, and somatomotor regions. State 8 was characterized by frontoinsular regions including coactivation of the anterior insula, and anterior regions of the canonical default network, including the medial prefrontal cortex and temporal pole. Displayed network states were normed (so that activation across the whole brain for that state was centered at zero).

Downloaded for Anonymous User (n/a) at Harvard University from ClinicalKey.com by Elsevier on September 15, 2022. For personal use only. No other uses without permission. Copyright ©2022. Elsevier Inc. All rights reserved.

reliability). State 1 included corticolimbic regions involved in emotion regulation and included coactivation of areas of the orbitofrontal and medial prefrontal cortices, temporal pole, and limbic regions. State 2 was characterized by coactive regions of the canonical DN and included midline cortical systems, angular gyrus, and middle temporal regions. State 3 consisted of coactivation among sensorimotor regions extending to the parahippocampal cortex and posterior parietal cortex. State 4 was characterized by coactivation of occipital and posterior parietal regions including the posterior cingulate. State 5 overlapped with ventral and posterior areas of the canonical affective network and DN, with coactivation of posterior cingulate, orbitofrontal, and limbic areas. State 6 was characterized by coactivation of midcingulate and parietal regions, including the posterior dorsal anterior cingulate cortex extending to the supplementary motor area, and the superior temporal gyrus. State 7 overlapped with anterior areas of the canonical SN, including the anterior insula and midcingulate, temporoparietal, and somatomotor regions. State 8 was characterized by coactivation of anterior frontoinsular regions that overlapped with the DN, including coactivation of the anterior insula, medial prefrontal cortex, lateral prefrontal cortex, and temporal pole.

Correlation analyses on dynamic measures between CAP states revealed shared dynamic patterns across network states. Specifically, states 1 and 3, states 2 and 7, states 4 and 8, and states 5 and 6 showed consistent patterns of positive correlations in time-in-state at baseline, in time-in-state at 1 week, and in changes in time-in-state (Table S3). Therefore, to reduce collinearity in subsequent models, dynamic measures (at baseline or changes in time-in-state) were z-transformed and averaged for each pair of network states with shared dynamic patterns. Following these transformations, correlations among composite scores were inspected and any composite scores showing high anticorrelations were combined by reverse scoring and averaging. Together, these procedures yielded the following dynamic variables for analyses: baseline time-in-states: 1/3, 2/7, 4/8, and 5/6; changes in time-in-states: 1/3, 2/5/6/7, and 4/8.

Effects of Time and Treatment on Depression Severity

A simple mixed effects model evaluated changes in depressive symptom severity over the 8-week period of treatment (Figure S2). Results showed significant linear ($F_{1,204}$ = 194.60, $p < .01$ [FDR $q < .01$]) and quadratic ($F_{1,204}$ = 59.91, $p < .01$ [FDR $q < .01$]) effects of time, in which HAMD scores decreased over time and leveled off in later weeks.

Antidepressant group was added to the model to evaluate whether decreases in depressive symptoms over the treatment period differed for patients receiving sertraline versus placebo (Figure S2). Results indicated that patients in the sertraline group showed steeper linear improvement in HAMD scores than patients in the placebo group ($F_{1,201}$ = 4.37, p = .04 [FDR q = .05]) but no difference in quadratic patterns of symptom change ($F_{1,201}$ = 0.35, p = .55). However, it is noted that the treatment-related differences in linear symptom improvement were relatively small (standardized $B = -0.06$).

Baseline Transient Network Dynamics and Depression Severity

The mixed effects model above was repeated including baseline time-in-state measures as moderators of the effects of treatment time, antidepressant group, and treatment time × group interaction. The model showed no significant associations between baseline time-in-CAP-states and initial depression or changes in depression over the study period, and baseline time-in-CAP-states did not moderate the relationship between treatment group and depression improvement (all p values $> .10$).

Changes in Transient Network Dynamics and Depression Severity

The mixed effects model was next repeated including changes in time-in-state measures as moderators of the effect of treatment time, controlling for baseline time-in-state and antidepressant group (Figure 2). Participants showing increasing time-in-states 1 and 3 reported nonsignificantly steeper (linear) declines in depression ($F_{1,190}$ = 2.96, p = .08 [FDR q = .09]) that more rapidly leveled off (quadratic) ($F_{1,190}$ = 5.48, p = .02 [FDR q = .03]). Participants showing increasing time-in-states 2 and 7 and decreasing time-in-states 5 and 6 reported significantly steeper (linear) declines in depression ($F_{1,190}$ = 6.25, p = .01 [FDR q = .03]) but no difference in quadratic patterns ($F_{1,190}$ = 0.64, p = .43). Finally, patients showing increasing time-in-states 4 and 8 reported comparable linear changes in depression ($F_{1,190}$ = 1.76, p = .18), but symptom improvement leveled off more rapidly, indicating failure to sustain this rate of improvement (quadratic) ($F_{1,190}$ = 4.04, p = .04 [FDR q = .05]) (see the Supplement for model cross-validation).

Mediation: Treatment Effects on Depression Through Changes in Transient Network Dynamics

Post hoc models were performed to evaluate indirect effects of sertraline on depression severity through early changes in network dynamics. Antidepressant treatment group failed to predict changes in time-in-states 1 and 3 ($F_{1,206}$ = 0.92, p = .92), and the indirect effect of treatment group on HAMD improvement through changes in states 1/3 was not significant (estimate = 0.014, bootstrapped 95% CI = −0.016 to 0.060). Patients across groups showed increased time-in-states 1 and 3 (Table S4).

However, relative to the placebo condition, patients receiving sertraline showed significantly greater increases in time-in-states 2 and 7 and decreases in time-in-states 5 and 6 ($F_{1,206}$ = 25.40, $p < .01$ [FDR $q < .01$]) (Figure 3). Mediation analyses revealed a significant indirect effect of sertraline treatment on symptoms through these patterns of network change (estimate = 0.060, 95% CI = 0.02 to 0.147) (Figure 4). Post hoc interrogation of these effects clarified that patients receiving sertraline especially showed increased time-in-state 2, and the indirect effect of sertraline on symptom improvement through increased time-in-state 2 was significant (estimate = 0.057, 95% CI = 0.010 to 0.145).

Finally, there was no significant difference between antidepressant groups in changes in time-in-states 4 and 8 ($F_{1,206}$ = 1.80, p = .23), and the indirect effect of sertraline on depressive

Downloaded for Anonymous User (n/a) at Harvard University from ClinicalKey.com by Elsevier on September 15, 2022. For personal use only. No other uses without permission. Copyright ©2022. Elsevier Inc. All rights reserved.

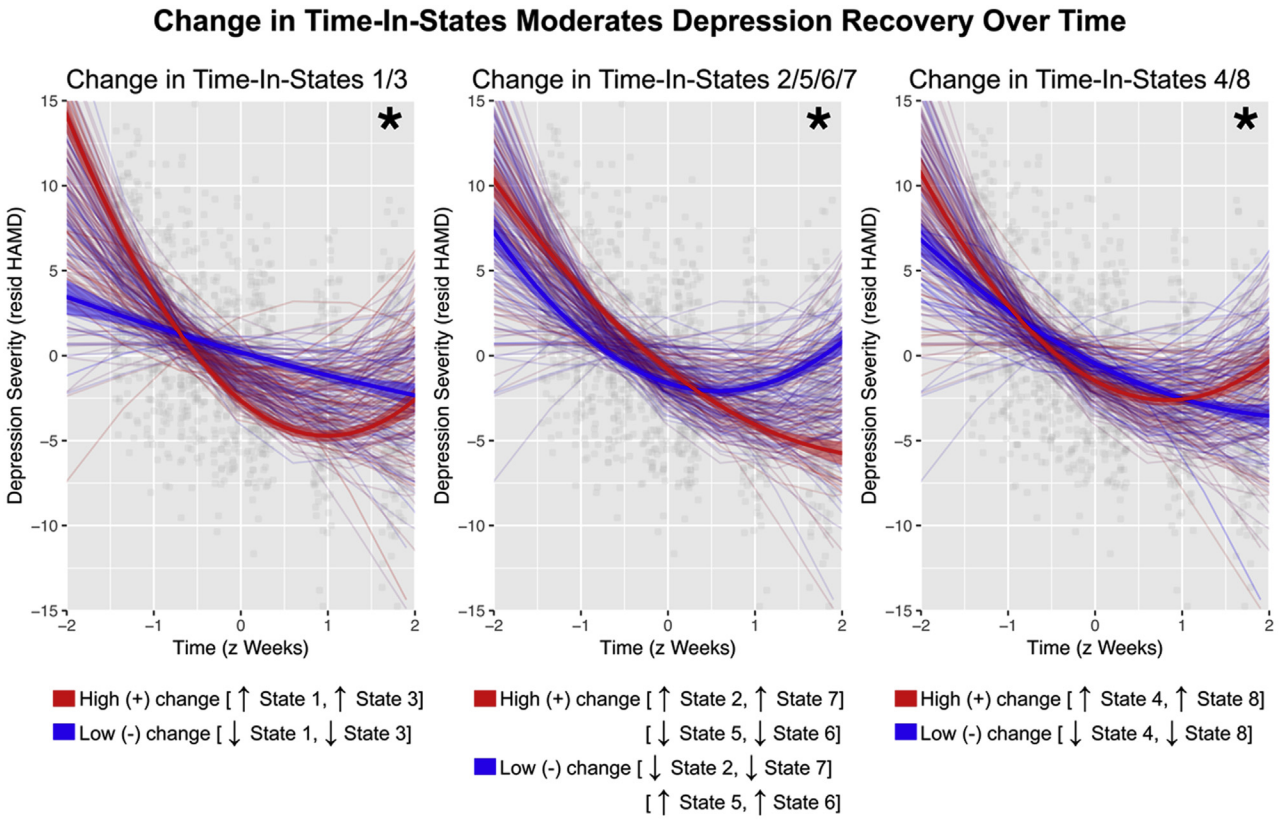

Figure 2. Early changes in network dynamics are associated with depression recovery over time. Patients showing early increases in time spent in network states 1 and 3 showed marginally steeper linear improvements in depressive symptom severity ($F_{1,190}$ = 2.96, p = .08) that leveled off more rapidly ($F_{1,190}$ = 5.48, p = .02). Patients showing early increases in time-in-states 2 and 7, together with decreases in time-in-states 5 and 6, showed significantly steeper linear improvement in depressive symptom severity that continued in later weeks of treatment ($F_{1,190}$ = 6.25, p = .01). Patients showing early increases in (or failure to decrease) time-in-states 4 and 8 showed a stronger quadratic pattern of symptom change in which symptoms leveled off or rebounded in later weeks of treatment ($F_{1,190}$ = 4.04, p = .04). Displayed are scatterplots showing Hamilton Depression Rating Scale (HAMD) scores for patients at all time points and curvilinear within-subject changes in depression severity. To illustrate the moderating effects of changes in network dynamics, fit lines are estimated and shown at more positive change in composite time-in-states (+2 standard deviations above median change, red) or more negative change in composite time-in-states (−2 standard deviations below median change, blue) for each set of states (note that time-in-states 5/6 is reverse-scored). HAMD score was residualized for covariates (age, gender, and baseline time-in-states) for graphical display. Time in weeks was z-scored, weeks 0–8. *$p < .05$, moderating effects of time-in-states on depression change over time. resid, residualized.

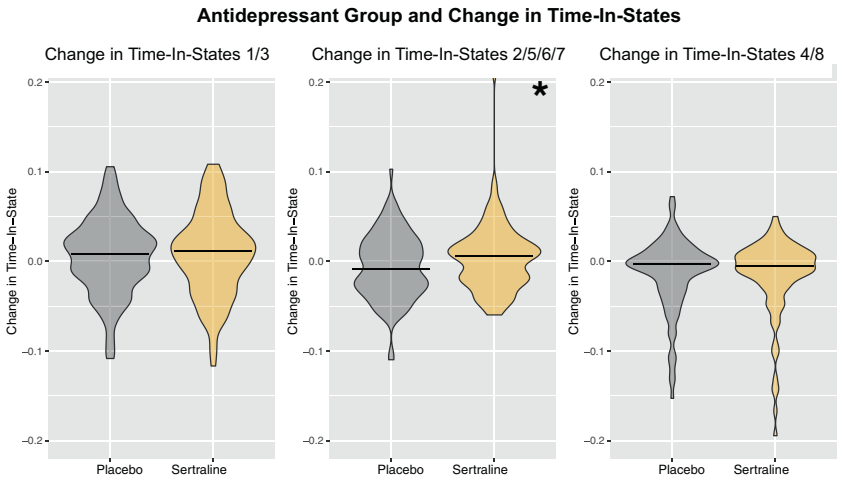

Figure 3. Antidepressant group differences in early changes in network dynamics. Relative to patients receiving placebo, patients receiving sertraline showed significantly greater increases in composite changes in time-in-states 2, 5, 6, and 7 ($F_{1,206}$ = 25.40, $p < .01$), indicating larger increases in time-in-states 2 and 7 and decreases in time-in-states 5 and 6. Post hoc testing indicated significant sertraline-related increases in time-in-state 2. There were no differences between antidepressant treatment groups in changes in time-in-states 1 and 3 or time-in-states 4 and 8. Violin plots show distributions of composite changes in time-in-state, with horizontal lines indicating median within-group changes. *$p < .05$, antidepressant group differences.

Downloaded for Anonymous User (n/a) at Harvard University from ClinicalKey.com by Elsevier on September 15, 2022. For personal use only. No other uses without permission. Copyright ©2022. Elsevier Inc. All rights reserved.

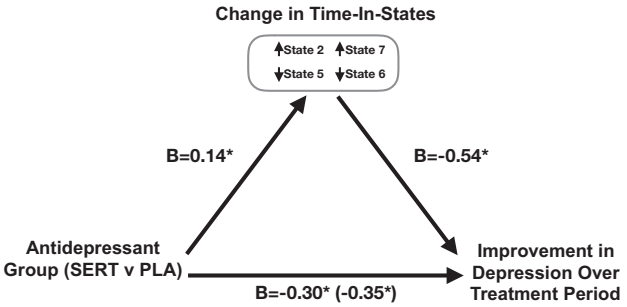

Figure 4. Indirect effect of sertraline (SERT) treatment on depression recovery through early changes in network dynamics. Significant mediated effects were observed (estimate = 0.060, 95% CI = 0.02 to 0.147) in which SERT treatment was associated with steeper linear improvement in depression through changes in network dynamics, including increased time-in-states that overlapped with the canonical default network and salience network (states 2 and 7) and decreased time-in-states that were characterized by mid- and posterior cingulate regions in coactivation with ventral limbic and temporal regions (states 5 and 6). Paths show standardized coefficients (B) for the association between antidepressant group and early changes in time-in-states; between early changes in time-in-states and linear improvement in Hamilton Depression scores, controlling for group; and between antidepressant group and linear improvement in Hamilton Depression scores, controlling for changes in time-in-states. *$p < .05$. PLA, placebo.

symptom change through changes in states 4/8 was nonsignificant (estimate = 0.003, 95% CI = 0.000 to 0.010). Patients across groups showed decreased time-in-states 4 and 8 (Table S4).

DISCUSSION

Identification of objective neural markers that forecast antidepressant response and recovery is a critical goal for precision medicine. This study aimed to address this goal, investigating dynamic resting-state network markers that moderated or mediated response to sertraline in a large sample of adults with MDD. The focus on dynamics of resting-state networks was motivated by evidence that such dynamics are reliable (21) and correspond with severity of illness and maladaptive cognitive style in depression (23); here, we extend prior work to understand network dynamics as predictors or mechanisms of antidepressant (and placebo) effects on symptomatology. Several key results emerged. First, network dynamics involving regions of (canonical) default network and salience network mediated sertraline-related symptom improvement, implying that dynamic functioning of these networks may serve as an indicator of treatment effect. Second, network dynamics involving corticolimbic and frontoinsular networks were broadly associated with patterns of symptom change but not antidepressant treatment, suggesting that dynamic functioning of these networks may more generally track with recovery. We note that, counter to our hypotheses, there were no significant associations between baseline network dynamics and treatment outcome, which stands in contrast to prior work on (static) resting-state functional connectivity markers [e.g., (30,31)]. It may be that static versus dynamic properties of network functioning hold different but complementary information to guide treatment research.

Sertraline response was associated with a pattern of changing dynamics across transient networks that closely matched canonical DN and SN (increased time-in-states 2 and 7) or that showed a spatial mixture of DN- or SN-like features (mid- and posterior cingulate) in coactivation with limbic and temporal regions (decreased time-in-states 5 and 6). Early changes in the dynamic functioning of these networks mediated the effects of sertraline on depression improvement. One interpretation of this pattern is that sertraline effectively sharpened network boundaries, eliciting increased dominance of states that more closely match canonical DN and SN states while dampening mixed states in which regions involved in introspection and salience-directed attention coactivate with affective and posterior regions. This interpretation aligns with prior work showing that the first week of SSRI administration elicits increases in extracellular serotonin in prefrontal and subcortical regions but decreases in extracellular serotonin in other frontal regions, i.e., starker contrasts in extracellular serotonin across regions that may correspond with sharper network boundaries (17). In turn, sharpening of network boundaries may be associated with other potential mechanisms of sertraline including better prefrontal regulation of subcortical systems (32) or long-term structural changes in prefrontal systems (33) [see related review in (34)]. Future research may explore the associations among sertraline-related neural changes.

The finding that resting-state networks related to canonical DN and SN are associated with treatment response aligns with prior work implicating these networks in the pathophysiology of depression (11,12,35), but it may seem counterintuitive that increased dominance of a DN-like network state was related to better outcomes given evidence for DN hyperconnectivity and hyperactivation in MDD (10,36). However, these results are consistent with evidence for spatially overlapping DNs and subnetworks that have different associations with depressive symptoms (23). For example, antidepressant response has been associated with higher resting-state activity in dorsal regions but lower resting-state activity in ventral regions of the anterior DN (14) and increases in regional synchrony of anterior regions of DN over the course of treatment (37). This fractionation of DN, which may relate to dynamic activities of multiple overlapping DN-like networks, is obscured in traditional static analyses. For example, here, we identified multiple transient networks that overlapped with canonical DN, including state 2 (a more prototypical DN-like state) and state 8 (a state featuring coactivation across anterior insula and medial prefrontal regions of DN). Whereas increased time in a prototypical DN state was an early marker that mediated better treatment response, decreased time in a frontoinsular-DN state was related to better recovery overall. The latter pattern is consistent with our prior research, in which a frontoinsular-DN state was related to more severe depression and the tendency to ruminate (23), and emphasizes the importance of dynamic approaches that make it possible to tease apart spatially overlapping transient networks.

Along with dynamic network markers of treatment response, this study also identified potential markers of recovery that were shared across treatment groups. Increased time spent in states 1 and 3 was associated with marginally more rapid symptom remission, which leveled off earlier in the

Downloaded for Anonymous User (n/a) at Harvard University from ClinicalKey.com by Elsevier on September 15, 2022. For personal use only. No other uses without permission. Copyright ©2022. Elsevier Inc. All rights reserved.

period of treatment. In turn, failure to decrease time spent in states 4 and 8 was associated with worse symptom remission, in the form of initially comparable linear gains that also leveled off earlier in the period of treatment (i.e., stalled recovery at a higher level of severity). Findings for a relationship between corticolimbic circuits involved in emotion regulation (state 1) and depression recovery are consistent with other research indicating that enhanced activity and synchrony of corticolimbic regions corresponds with affective change within person (38), is elicited by SSRI administration (17), and predicts or tracks with SSRI response in MDD (11). In addition, as noted above, findings for a depressogenic effect of frontoinsular-DN (state 8) dominance are consistent with prior evidence that greater dominance of a similar network state was associated with higher depression (23). Here, these network dynamics were associated with patterns of symptom change and were not significantly associated with medication status. It may be that corticolimbic and frontoinsular-DN circuits constitute general biomarkers that help to predict particular patterns of depression recovery, irrespective of whether recovery is associated with medication, placebo, or the passage of time.

Some limitations to this study should be noted. First, the generalizability of results is limited to patient populations that match the eligibility, demographic, and treatment-adherence characteristics of this study. Other research should explore biomarkers of antidepressant response in community or primary care settings or in other demographic or developmental groups. Second, it is unknown whether resting-state mediators of sertraline response are shared or distinct from those of other antidepressant medications or therapies. Studies comparing biomarkers across interventions, and replicability or relative utility of biomarkers related to interventions or general recovery, may test this question. Third, the use of a novel dynamic method for identifying resting-state markers is both a strength of this study and a limitation. The data-driven approach made it possible to extract transient network states without imposing a spatial network organization, and this approach has been shown to have good test-retest reliability (21). In addition, these results align with other analyses using standard resting-state functional connectivity methods in the same sample (30). However, in light of concerns regarding the reliability of widely used neuroimaging measures (39) and the relative novelty of dynamic approaches, these results should be replicated.

In conclusion, this study investigated novel dynamic resting-state network markers of treatment response in a randomized, placebo-controlled trial of sertraline response in adults with MDD. Key findings included identification of transient networks involving canonical default and salience regions, in which early functional changes mediated sertraline response, and a set of networks involving corticolimbic and frontoinsular regions that predicted general patterns of recovery from depression. Dynamic characteristics of resting-state network function may hold promise as biomarkers of early treatment efficacy, and future research in this area may further clinical and translational goals for precision medicine.

ACKNOWLEDGMENTS AND DISCLOSURES

The EMBARC study was supported by the National Institute of Mental Health (NIMH) (Grant Nos. U01MH092221 [to MHT] and U01MH092250 [to PJM, RVP, and MW]). RHK was partially supported by NIMH Grant No. R01MH117131.

In the last 3 years, the authors report the following financial disclosures for activities unrelated to this research:

MLP: funding from NIMH, the Brain and Behavior Research Foundation, and the Pittsburgh Foundation.

MF: lifetime disclosures: *Research Support:* Abbott Laboratories; Acadia Pharmaceuticals; Alkermes, Inc.; American Cyanamid; Aspect Medical Systems; AstraZeneca; Avanir Pharmaceuticals; AXSOME Therapeutics; BioClinica, Inc; Biohaven; BioResearch; BrainCells Inc.; Bristol-Myers Squibb; CeNeRx BioPharma; Centrexion Therapeutics Corporation; Cephalon; Cerecor; Clarus Funds; Clexio Biosciences; Clintara, LLC; Covance; Covidien; Eli Lilly and Company;EnVivo Pharmaceuticals, Inc.; Euthymics Bioscience, Inc.; Forest Pharmaceuticals, Inc.; FORUM Pharmaceuticals; Ganeden Biotech, Inc.; Gentelon, LLC; GlaxoSmithKline; Harvard Clinical Research Institute; Hoffman-LaRoche; Icon Clinical Research; Indivior; i3 Innovus/Ingenix; Janssen R&D, LLC; Jed Foundation; Johnson & Johnson Pharmaceutical Research & Development; Lichtwer Pharma GmbH; Lorex Pharmaceuticals; Lundbeck Inc.; Marinus Pharmaceuticals; MedAvante; Methylation Sciences Inc; National Alliance for Research on Schizophrenia & Depression (NARSAD); National Center for Complementary and Alternative Medicine (NCCAM); National Coordinating Center for Integrated Medicine (NiiCM); National Institute of Drug Abuse (NIDA); National Institutes of Health; National Institute of Mental Health (NIMH); Neuralstem, Inc.; NeuroRx; Novartis AG; Novaremed; Organon Pharmaceuticals; Otsuka Pharmaceutical Development, Inc.; PamLab, LLC.; Pfizer Inc.; Pharmacia-Upjohn; Pharmaceutical Research Associates., Inc.; Pharmavite® LLC; PharmoRx Therapeutics; Photothera; Praxis Precision Medicines; Premiere Research International; Protagenic Therapeutics, Inc.; Reckitt Benckiser; Relmada Therapeutics Inc.; Roche Pharmaceuticals; RCT Logic, LLC (formerly Clinical Trials Solutions, LLC); Sanofi-Aventis US LLC; Shenox Pharmaceuticals, LLC; Shire; Solvay Pharmaceuticals, Inc.; Stanley Medical Research Institute (SMRI); Synthelabo; Taisho Pharmaceuticals; Takeda Pharmaceuticals; Tal Medical; VistaGen; WinSanTor, Inc.; Wyeth- Ayerst Laboratories; *Advisory Board/Consultant:* Abbott Laboratories; Acadia; Aditum Bio Management Company, LLC; Affectis Pharmaceuticals AG; Alfasigma USA, Inc.; Alkermes, Inc.; Altimate Health Corporation; Amarin Pharma Inc.; Amorsa Therapeutics, Inc.; Ancora Bio, Inc.; Angelini S.p.A; Aptinyx Inc.; Arbor Pharmaceuticals, LLC; Aspect Medical Systems; Astella Pharma Global Development, Inc.; AstraZeneca; Auspex Pharmaceuticals; Avanir Pharmaceuticals; AXSOME Therapeutics; Bayer AG; Best Practice Project Management, Inc.; Biogen; BioMarin Pharmaceuticals, Inc.; BioXcel Therapeutics; Biovail Corporation; Boehringer Ingelheim; Boston Pharmaceuticals; BrainCells Inc; Bristol-Myers Squibb; Cambridge Science Corporation; CeNeRx BioPharma; Cephalon, Inc.; Cerecor; Clexio Biosciences; Click Therapeutics, Inc; CNS Response, Inc.; Compellis Pharmaceuticals; Cybin Corporation; Cypress Pharmaceutical, Inc.; DiagnoSearch Life Sciences (P) Ltd.; Dainippon Sumitomo Pharma Co. Inc.; Dr. Katz, Inc.; Dov Pharmaceuticals, Inc.; Edgemont Pharmaceuticals, Inc.; Eisai Inc.; Eli Lilly and Company; ElMindA; EnVivo Pharmaceuticals, Inc.; Enzymotec LTD; ePharmaSolutions; EPIX Pharmaceuticals, Inc.; Esthismos Research, Inc.; Euthymics Bioscience, Inc.; Evecxia Therapeutics, Inc.; ExpertConnect, LLC; FAAH Research Inc.; Fabre-Kramer Pharmaceuticals, Inc.; Forest Pharmaceuticals, Inc.; Forum Pharmaceuticals; Gate Neurosciences, Inc.; GenetikaPlus Ltd.; GenOmind, LLC; GlaxoSmithKline; Grunenthal GmbH; Happify; H. Lundbeck A/S; Indivior; i3 Innovus/Ingenis; Intracellular; Janssen Pharmaceutica; Jazz Pharmaceuticals, Inc.; JDS Therapeutics, LLC; Johnson & Johnson Pharmaceutical Research & Development, LLC; Knoll Pharmaceuticals Corp.; Labopharm Inc.; Lorex Pharmaceuticals; Lundbeck Inc.; Marinus Pharmaceuticals; MedAvante, Inc.; Merck & Co., Inc.; Mind Medicine Inc.; MSI Methylation Sciences, Inc.; Naurex, Inc.; Navitor Pharmaceuticals, Inc.; Nestle Health Sciences; Neuralstem, Inc.; Neurocrine Biosciences, Inc.; Neuronetics, Inc.; NextWave Pharmaceuticals; Niraxx Light Therapeutics, Inc; Northwestern University; Novartis AG; Nutrition 21; Opiant Pharmecuticals; Orexigen Therapeutics, Inc.; Organon Pharmaceuticals; Osmotica; Otsuka Pharmaceuticals; Ovid Therapeutics, Inc.; Pamlab, LLC.; Perception Neuroscience; Pfizer Inc.; PharmaStar; PharmaTher Inc.; Pharmavite® LLC.; PharmoRx Therapeutics; Polaris Partners; Praxis Precision Medicines; Precision Human Biolaboratory; Prexa Pharmaceuticals,

Downloaded for Anonymous User (n/a) at Harvard University from ClinicalKey.com by Elsevier on September 15, 2022. For personal use only. No other uses without permission. Copyright ©2022. Elsevier Inc. All rights reserved.

Inc.; Protagenic Therapeutics, Inc; PPD; PThera, LLC; Purdue Pharma; Puretech Ventures; Pure Tech LYT, Inc.; PsychoGenics; Psylin Neurosciences, Inc.; RCT Logic, LLC (formerly Clinical Trials Solutions, LLC); Relmada Therapeutics, Inc.; Rexahn Pharmaceuticals, Inc.; Ridge Diagnostics, Inc.; Roche; Sanofi-Aventis US LLC.; Sensorium Therapeutics; Sentier Therapeutics; Sepracor Inc.; Servier Laboratories; Schering-Plough Corporation; Shenox Pharmaceuticals, LLC; Solvay Pharmaceuticals, Inc.; Somaxon Pharmaceuticals, Inc.; Somerset Pharmaceuticals, Inc.; Sonde Health; Sunovion Pharmaceuticals; Supernus Pharmaceuticals, Inc.; Synthelabo; Taisho Pharmaceuticals; Takeda Pharmaceutical Company Limited; Tal Medical, Inc.; Tetragenex; Teva Pharmaceuticals; TransForm Pharmaceuticals, Inc.; Transcept Pharmaceuticals, Inc.; University of Michigan, Department of Psychiatry; Usona Institute,Inc.; Vanda Pharmaceuticals, Inc.; Versant Venture Management, LLC; VistaGen; Xenon Pharmaceuticals Inc.; *Speaking/Publishing:* Adamed, Co; Advanced Meeting Partners; American Psychiatric Association; American Society of Clinical Psychopharmacology; AstraZeneca; Belvoir Media Group; Boehringer Ingelheim GmbH; Bristol-Myers Squibb; Cephalon, Inc.; CME Institute/Physicians Postgraduate Press, Inc.; Eli Lilly and Company; Forest Pharmaceuticals, Inc.; GlaxoSmithKline; Global Medical Education, Inc.; Imedex, LLC; MGH Psychiatry Academy/Primedia; MGH Psychiatry Academy/Reed Elsevier; Novartis AG; Organon Pharmaceuticals; Pfizer Inc.; PharmaStar; United BioSource,Corp.; Wyeth-Ayerst Laboratories; *Equity Holdings*: Compellis; Neuromity; Psy Therapeutics; Sensorium Therapeutics; *Royalty/patent, other income*: Patents for Sequential Parallel Comparison Design (SPCD), licensed by MGH to Pharmaceutical Product Development, LLC (PPD) (US_7840419, US_7647235, US_7983936, US_8145504, US_8145505); and patent application for a combination of Ketamine plus Scopolamine in Major Depressive Disorder (MDD), licensed by MGH to Biohaven. Patents for pharmacogenomics of Depression Treatment with Folate (US_9546401, US_9540691). *Copyright:* for the MGH Cognitive & Physical Functioning Questionnaire (CPFQ), Sexual Functioning Inventory (SFI), Antidepressant Treatment Response Questionnaire (ATRQ), Discontinuation-Emergent Signs & Symptoms (DESS), Symptoms of Depression Questionnaire (SDQ), and SAFER; Belvoir; Lippincott, Williams & Wilkins; Wolkers Kluwer; World Scientific Publishing Co. Pte. Ltd.

MW: funding from NIMH, the National Alliance for Research on Schizophrenia and Depression, the Sackler Foundation, and the Templeton Foundation; royalties from Oxford University Press, Perseus Press, the American Psychiatric Association Press, and Multi-Health Systems.

MAO: funding from NIMH; royalties from the Research Foundation for Mental Hygiene for the commercial use of the Columbia Suicide Severity Rating Scale and shares in Mantra, Inc.; adviser to Alkermes, Otsuka, ATAI, St George's University, and Fundación Jiménez Díaz. Her family owns stock in Bristol-Myers Squibb.

MGM: funding from NIMH; consulting fees from Janssen and Otsuka Pharmaceuticals.

TC: owns stock in Vertex Pharmaceuticals and CRISPR Therapeutics.

MHT: research support from the Agency for Healthcare Research and Quality, Cyberonics Inc., National Alliance for Research in Schizophrenia and Depression, NIMH, National Institute on Drug Abuse, National Institute of Diabetes and Digestive and Kidney Diseases, and Johnson & Johnson; consulting and speaker fees from Abbott Laboratories Inc., Akzo (Organon Pharmaceuticals Inc.), Allergan Sales LLC, Alkermes, Astra Zeneca, Axon Advisors, Brintellix, Bristol-Myers Squibb Company, Cephalon Inc., Cerecor, Eli Lilly & Company, Evotec, Fabre Kramer Pharmaceuticals Inc., Forest Pharmaceuticals, GlaxoSmithKline, Health Research Associates, Johnson & Johnson, Lundbeck, MedAvante Medscape, Medtronic, Merck, Mitsubishi Tanabe Pharma Development America Inc., MSI Methylation Sciences Inc., Nestle Health Science-PamLab Inc., Naurex, Neuronetics, One Carbon Therapeutics Ltd, Otsuka Pharmaceuticals, Pamlab, Parke-Davis Pharmaceuticals Inc., Pfizer Inc., PgxHealth, Phoenix Marketing Solutions, Rexahn Pharmaceuticals, Ridge Diagnostics, Roche Products Ltd, Sepracor, SHIRE Development, Sierra, SK Life and Science, Sunovion, Takeda, Tal Medical/Puretech Venture, Targacept, Transcept, VantagePoint, Vivus, and Wyeth-Ayerst Laboratories.

DAP: funding from NIMH, Brain and Behavior Research Foundation, the Dana Foundation, and Millennium Pharmaceuticals; consulting fees from Neumora Therapeutics (formerly BlackThorn Therapeutics), Boehringer Ingelheim (Ingelheim, Germany), Compass Pathways, Concert Pharmaceuticals, Engrail Therapeutics, Neurocrine Biosciences, Neuroscience Software, Otsuka Pharmaceuticals, and Takeda Pharmaceuticals; honoraria from the Psychonomic Society (for editorial work) and Alkermes; stock options from Neumora Therapeutics (formerly BlackThorn Therapeutics), Compass Pathways, and Neuroscience Software.

All other authors report no biomedical financial interests or potential conflicts of interest. No funding from these entities was used to support this work, and all views expressed are solely those of the authors.

ARTICLE INFORMATION

From the Department of Psychology and Neuroscience (RHK), Institute of Cognitive Science (RHK), and Renée Crown Wellness Institute (RHK), University of Colorado Boulder, Boulder, Colorado; Department of Psychiatry (HWC, MLP), University of Pittsburgh, Pittsburgh, Pennsylvania; Department of Psychiatry (TD, MF), Harvard Medical School and Massachusetts General Hospital; Department of Psychiatry (DAP), Harvard Medical School and McLean Hospital, Boston, Massachusetts; Department of Psychiatry (RVP), Stony Brook University, Stony Brook; Department of Psychiatry, New York State Psychiatric Institute and Columbia University Vagelos College of Physicians and Surgeons (PJM, MW), New York, New York; Department of Psychiatry (MAO), Perelman School of Medicine, University of Pennsylvania, Philadelphia, Pennsylvania; Department of Psychiatry (MGM), University of Michigan, Ann Arbor, Michigan; and the Department of Psychiatry (TC, CMC, MHT), University of Texas, Southwestern Medical Center, Dallas, Texas

Address correspondence to Roselinde H. Kaiser, Ph.D., at Roselinde.Kaiser@colorado.edu.

Received Nov 15, 2021; revised Mar 2, 2022; accepted Mar 23, 2022.

Supplementary material cited in this article is available online at https://doi.org/10.1016/j.biopsych.2022.03.020.

REFERENCES

1. Farmer RF, Kosty DB, Seeley JR, Olino TM, Lewinsohn PM (2013): Aggregation of lifetime Axis I psychiatric disorders through age 30: Incidence, predictors, and associated psychosocial outcomes. J Abnorm Psychol 122:573–586.
2. Kessler RC, Petukhova M, Sampson NA, Zaslavsky AM, Wittchen HU (2012): Twelve-month and lifetime prevalence and lifetime morbid risk of anxiety and mood disorders in the United States. Int J Methods Psychiatr Res 21:169–184.
3. Ferrari AJ, Charlson FJ, Norman RE, Patten SB, Freedman G, Murray CJL, *et al.* (2013): Burden of depressive disorders by country, sex, age, and year: Findings from the global burden of disease Study 2010. PLoS Med 10:e1001547.
4. Walker ER, McGee RE, Druss BG (2015): Mortality in mental disorders and global disease burden implications: A systematic review and meta-analysis [published correction appears in JAMA Psychiatry 2015; 72:736] [published correction appears in JAMA Psychiatry 2015; 72: 1259]. JAMA Psychiatry 72:334–341.
5. Moore TJ, Mattison DR (2017): Adult utilization of psychiatric drugs and differences by sex, age, and race [published correction appears in JAMA Intern Med 2017; 177:449]. JAMA Intern Med 177:274–275.
6. Trivedi MH, Rush AJ, Wisniewski SR, Nierenberg AA, Warden D, Ritz L, *et al.* (2006): Evaluation of outcomes with citalopram for depression using measurement-based care in STAR*D: Implications for clinical practice. Am J Psychiatry 163:28–40.
7. McIntyre RS, O'Donovan C (2004): The human cost of not achieving full remission in depression. Can J Psychiatry 49(suppl 1):10S–16S.
8. Lenze EJ, Rodebaugh TL, Nicol GE (2020): A framework for advancing precision medicine in clinical trials for mental disorders [published correction appears in JAMA Psychiatry 2020; 77:768]. JAMA Psychiatry 77:663–664.
9. Buckner RL, Krienen FM, Yeo BTT (2013): Opportunities and limitations of intrinsic functional connectivity MRI. Nat Neurosci 16:832–837.

Downloaded for Anonymous User (n/a) at Harvard University from ClinicalKey.com by Elsevier on September 15, 2022. For personal use only. No other uses without permission. Copyright ©2022. Elsevier Inc. All rights reserved.

10. Kaiser RH, Andrews-Hanna JR, Wager TD, Pizzagalli DA (2015): Large-scale network dysfunction in major depressive disorder: A meta-analysis of resting-state functional connectivity. JAMA Psychiatry 72:603–611.
11. Dichter GS, Gibbs D, Smoski MJ (2015): A systematic review of relations between resting-state functional-MRI and treatment response in major depressive disorder. J Affect Disord 172:8–17.
12. Brakowski J, Spinelli S, Dörig N, Bosch OG, Manoliu A, Holtforth MG, Seifritz E (2017): Resting state brain network function in major depression—Depression symptomatology, antidepressant treatment effects, future research. J Psychiatr Res 92:147–159.
13. Long Z, Du L, Zhao J, Wu S, Zheng Q, Lei X (2020): Prediction on treatment improvement in depression with resting state connectivity: A coordinate-based meta-analysis. J Affect Disord 276:62–68.
14. Emam H, Steffens DC, Pearlson GD, Wang L (2019): Increased ventromedial prefrontal cortex activity and connectivity predict poor sertraline treatment outcome in late-life depression. Int J Geriatr Psychiatry 34:730–737.
15. Dunlop BW, Rajendra JK, Craighead WE, Kelley ME, McGrath CL, Choi KS, *et al.* (2017): Functional connectivity of the subcallosal cingulate cortex and differential outcomes to treatment with cognitive-behavioral therapy or antidepressant medication for major depressive disorder [published correction appears in Am J Psychiatry 2017; 174: 604]. Am J Psychiatry 174:533–545.
16. Crowther A, Smoski MJ, Minkel J, Moore T, Gibbs D, Petty C, *et al.* (2015): Resting-state connectivity predictors of response to psychotherapy in major depressive disorder. Neuropsychopharmacology 40:1659–1673.
17. Fritze S, Spanagel R, Noori HR (2017): Adaptive dynamics of the 5-HT systems following chronic administration of selective serotonin reuptake inhibitors: A meta-analysis. J Neurochem 142:747–755.
18. Kraus C, Ganger S, Losak J, Hahn A, Savli M, Kranz GS, *et al.* (2014): Gray matter and intrinsic network changes in the posterior cingulate cortex after selective serotonin reuptake inhibitor intake. Neuroimage 84:236–244.
19. Taylor MJ, Freemantle N, Geddes JR, Bhagwagar Z (2006): Early onset of selective serotonin reuptake inhibitor antidepressant action: Systematic review and meta-analysis. Arch Gen Psychiatry 63:1217–1223.
20. Kaiser RH, Snyder HR, Goer F, Clegg R, Ironside M, Pizzagalli DA (2018): Attention bias in rumination and depression: Cognitive mechanisms and brain networks. Clin Psychol Sci 6:765–782.
21. Janes AC, Peechatka AL, Frederick BB, Kaiser RH (2020): Dynamic functioning of transient resting-state coactivation networks in the Human Connectome Project. Hum Brain Mapp 41:373–387.
22. Kaiser RH, Whitfield-Gabrieli S, Dillon DG, Goer F, Beltzer M, Minkel J, *et al.* (2016): Dynamic resting-state functional connectivity in major depression. Neuropsychopharmacology 41:1822–1830.
23. Kaiser RH, Kang MS, Lew Y, Van Der Feen J, Aguirre B, Clegg R, *et al.* (2019): Abnormal frontoinsular-default network dynamics in adolescent depression and rumination: A preliminary resting-state co-activation pattern analysis. Neuropsychopharmacology 44:1604–1612.
24. Ang YS, Kaiser R, Deckersbach T, Almeida J, Phillips ML, Chase HW, *et al.* (2020): Pretreatment reward sensitivity and frontostriatal resting-state functional connectivity are associated with response to bupropion after sertraline nonresponse. Biol Psychiatry 88:657–667.
25. Trivedi MH, McGrath PJ, Fava M, Parsey RV, Kurian BT, Phillips ML, *et al.* (2016): Establishing moderators and biosignatures of antidepressant response in clinical care (EMBARC): Rationale and design. J Psychiatr Res 78:11–23.
26. Hamilton M (1960): A rating scale for depression. J Neurol Neurosurg Psychiatry 23:56–62.
27. Yeo BTT, Krienen FM, Sepulcre J, Sabuncu MR, Lashkari D, Hollinshead M, *et al.* (2011): The organization of the human cerebral cortex estimated by intrinsic functional connectivity. J Neurophysiol 106:1125–1165.
28. Choi EY, Yeo BTT, Buckner RL (2012): The organization of the human striatum estimated by intrinsic functional connectivity. J Neurophysiol 108:2242–2263.
29. Liu X, Duyn JH (2013): Time-varying functional network information extracted from brief instances of spontaneous brain activity. Proc Natl Acad Sci U S A 110:4392–4397.
30. Chin Fatt CR, Jha MK, Cooper CM, Fonzo G, South C, Grannemann B, *et al.* (2020): Effect of intrinsic patterns of functional brain connectivity in moderating antidepressant treatment response in major depression. Am J Psychiatry 177:143–154.
31. Korgaonkar MS, Goldstein-Piekarski AN, Fornito A, Williams LM (2020): Intrinsic connectomes are a predictive biomarker of remission in major depressive disorder. Mol Psychiatry 25:1537–1549.
32. Anand A, Li Y, Wang Y, Gardner K, Lowe MJ (2007): Reciprocal effects of antidepressant treatment on activity and connectivity of the mood regulating circuit: An fMRI study. J Neuropsychiatry Clin Neurosci 19:274–282.
33. Willard SL, Uberseder B, Clark A, Daunais JB, Johnston WD, Neely D, *et al.* (2015): Long term sertraline effects on neural structures in depressed and nondepressed adult female nonhuman primates. Neuropharmacology 99:369–378.
34. Wandschneider B, Koepp MJ (2016): Pharmaco fMRI: Determining the functional anatomy of the effects of medication. Neuroimage Clin 12:691–697.
35. Gudayol-Ferré E, Peró-Cebollero M, González-Garrido AA, Guàrdia-Olmos J (2015): Changes in brain connectivity related to the treatment of depression measured through fMRI: A systematic review. Front Hum Neurosci 9:582.
36. Kaiser RH, Andrews-Hanna JR, Spielberg JM, Warren SL, Sutton BP, Miller GA, *et al.* (2015): Distracted and down: Neural mechanisms of affective interference in subclinical depression. Soc Cogn Affect Neurosci 10:654–663.
37. Lai CH (2011): Duloxetine's effects in resting functional magnetic resonance imaging of first-episode, drug-naive major depressive disorder with panic disorder patients. J Neuropsychiatry Clin Neurosci 23:E10–E11.
38. Phillips ML, Schmithorst VJ, Banihashemi L, Taylor M, Samolyk A, Northrup JB, *et al.* (2021): Patterns of infant amygdala connectivity mediate the impact of high caregiver affect on reducing infant smiling: Discovery and replication. Biol Psychiatry 90:342–352.
39. Elliott ML, Knodt AR, Ireland D, Morris ML, Poulton R, Ramrakha S, *et al.* (2020): What is the test-retest reliability of common task-functional MRI measures? New empirical evidence and a meta-analysis Psychol Sci 31:792–806.

Downloaded for Anonymous User (n/a) at Harvard University from ClinicalKey.com by Elsevier on September 15, 2022. For personal use only. No other uses without permission. Copyright ©2022. Elsevier Inc. All rights reserved.

Supplementary Information:

Dynamic Resting-State Network Biomarkers of Antidepressant Treatment Response

Supplementary Methods

Analyses

General image preprocessing. Functional data were preprocessed using Statistical Parametric Mapping 12 (SPM12, http://www.fil.ion.ucl.ac.uk/spm/software/spm12/) with the standard spatial preprocessing steps of slice-time correction, realignment, segmentation, normalization in Montreal Neurological Institute (MNI) space, and smoothing with a 6-mm kernel.

Regions of interest. Cortical and striatal regions of interest were defined by a publicly available parcellation map that is based on functionally coupled regions in 500 healthy adult subjects and was replicated in an independent sample of 500 healthy adult subjects (1,2). Subcortical limbic regions were defined by the AAL atlas. There were a total of 130 ROIs in the spatial map. We (3–5) and others (6) have used the same spatial ROI map in prior co-activation pattern analyses. We note that prior research comparing CAP states derived using different ROI maps (including a map using the network parcellation used here from (1)) showed good spatial reproducibility of CAPs across parcellations (7).

Motion thresholding and exclusions. We used SPM12 (http://www.fil.ion.ucl.ac.uk/spm/software/spm12/) to evaluate head motion by translation and rotation in *x, y, z* directions, and Artifact Detection Tools (ART, www.nitrc.org/projects/artifact_detect/) to calculate time points of significant head motion or fluctuations in the magnetic field (>0.5 mm motion from previous frame, global mean intensity >3 standard deviations from mean intensity across functional scans) for each participant. For any scan in which high levels of motion or artifacts across the time series was observed (>15% of volumes contaminated by motion or artifact, according to the thresholds above), that scan was

excluded from subsequent analyses. After these exclusions, *n*=259 eligible baseline resting-state scan series, and *n*=229 eligible week 1 resting-state scan series, were retained.

Co-activation pattern analysis. As reported in the main text, *k*s of 5 to 11 were tested. This range was selected based on prior evidence that reliable dominant co-activation patterns were detected in resting-state and task fMRI data in this range, but not at $k \leq 4$ or $k \geq 12$ (8).

Supplementary Results

Coactivation Pattern Analysis (CAP): Quality Controls and Reliability

Information on the spatial organization of CAP-derived transient network states is reported in the main text.

Descriptive statistics. Descriptive statistics for CAP states are reported in Supplementary Tables. Any CAP states showing high skew and kurtosis (states 4 and 8; Table S2) were natural-log transformed[1] before subsequent analyses.

Cluster cohesion. To test cluster cohesion, we calculated silhouette scores (a measure of how similar each volume of data is to the cluster in which it is grouped) for each co-activation state. Ranges of silhouette scores were comparable to other research using CAP analysis (3,4).

Motion checks. To compare brain states with motion estimates, we calculated the average framewise displacement associated with each brain state and there was no evidence that any brain states were contaminated by motion (average framewise displacement <0.2mm for all states). To further evaluate potential associations between motion and specific CAP states, we tested for differences between CAP states on average framewise displacement (mean FWD is

[1] An alternative transformation for proportion data is the arcsine transformation (although this has been critiqued (9)). Exploratory testing of the arcsine transformation as an alternative indicated that arcsine transformation performed more poorly in correcting skew and kurtosis in these data, therefore we retained natural-log transformation.

reported in Table S2). There were no differences between CAP states in motion (ps>0.05, Figure S3).

As an additional check, we censored the timeseries for each participant at a conservative threshold (movement >0.3mm) and tested whether there were differences in time-in-states between the censored and uncensored timeseries. There were no significant changes in time-in-states for any CAP state after censoring (ps>0.05). In addition, we tested the reliability of time-in-states across the censored and uncensored timeseries by correlating time-in-states estimates derived from censored and uncensored data. Correlations between proportional time-in-states of the censored relative to uncensored timeseries ranged from r=0.97 to r=0.99, (Figure S3), indicating that individual differences in time-in-states were stable across censored and uncensored data. Together, these control analyses support that CAP states and time-in-state measures were robust to motion.

Finally, we repeated group-level mixed effects analyses controlling for data quality (volumes affected by motion or spikes in global signal). The results of these augmented models were consistent with models reported in the main text, i.e., no changes in the nature or significance of any effects (changes in ps<0.002).

State frequency checks. We evaluated the timing of CAP states over the timeseries by estimating the interval between recurrences of each state. If one or more CAP states tended to recur at frequencies that are associated with noise signals (e.g., respiration, 0.1-0.5 Hz, cardiac activity, 0.6-1.2 Hz, drift, <0.008 Hz (10)), this could suggest that activity of this CAP state is driven by non-neuronal processes.

On average across participants and over the timeseries, the mean interval between state recurrences ranged from 7.17 to 33.54 volumes (14.43 to 67.08 seconds per cycle, or 0.015 to

0.070 Hz) (Figure S4). Average recurrence frequencies for all states fell within the standard band-pass filter for resting-state functional connectivity analyses, of 0.008 to 0.090 Hz (11), and are below high-frequency signals related to cardiac or respiratory activity (10) or low-frequency signals related to scanner drift.

Comparing spatial organization of CAP states across samples. Reliability of the spatial organization of CAP states was evaluated by comparing the spatial organization of the eight CAP states detected in this sample with the spatial organization of the eight CAP states that were reported in a sample of participants from the Human Connectome Project using the same methods for deriving co-activation patterns (HCP; (4)). Spatial overlap was computed in the form of Dice similarity coefficients, in which values approaching 1.0 indicate high spatial consistency in co-active regions. Results showed high levels of spatial overlap between network states estimated in the present sample and network states that were independently estimated in the HCP sample (Table S5). (See also (4) for additional analyses showing high reliability of spatial network organization within-subject in the HCP sample). Comparing across samples, three out of eight CAP states in the present study showed Dice coefficients >0.80 with states derived from the HCP dataset, and seven out of eight CAP states in the present study showed Dice coefficients >0.70 with states derived from the HCP dataset.

Of note, three states derived in the present sample showed spatial overlap >0.70 with more than one HCP state. State 2 in this study (corresponding with the canonical default network) showed highest overlap with HCP state 3, but also high overlap with 1. State 3 in this study (characterized by activation in sensorimotor and temporal regions) showed highest overlap with HCP state 6, but also high overlap with 4. State 7 in this study (corresponding with the canonical salience network) showed highest overlap with HCP state 5, but also high overlap with

4. These patterns are consistent with the finding (both here and within the HCP dataset), that there are multiple e.g., default network-like and salience network-like states with overlapping spatial characteristics. However, these findings also point to the complexity of comparing transient networks across samples: there was not a one-to-one match for all networks derived from the present sample and the HCP sample, and one state failed to show a Dice coefficient >0.70 with any HCP state. Differences may stem from differences in transient networks that characterize depressed compared with healthy individuals, but also highlight the importance of replication within a population.

Simulated data. We tested whether CAP network states could be detected in a simulated dataset, and whether network states derived from real data would outperform states derived from simulated data. Simulated data were created from the real dataset by shuffling the timeseries of activation of each ROI with respect to other ROIs (random shuffle of 1:length(vols)), but maintaining the integrity of the timeseries within each ROI. Next, the same approach to co-activation pattern analysis that is described in the main text was performed on the simulated data, with a k=8 clustering solution.

Silhouette scores for CAP states derived from simulated data versus real data were compared. It is noted that silhouette scores tend to be lower in higher-dimensional data (12); therefore, because the simulated data retained all characteristics of real data except for true patterns of spatial co-activation, this provides a useful benchmark for interpreting cluster cohesion. Results showed that across participants, silhouette scores were significantly higher for real data CAP states than for simulated data CAP states, $t(228)=62.30$, $p<0.01$, (Fig S5). In real data, average silhouette scores for each cluster ranged from 0.03-0.15, whereas in simulated data silhouette scores were <0.01 for all clusters.

Spatial overlap was computed between simulated data CAP states and states derived in the independent HCP sample (4), and compared with the estimates of spatial overlap between real data CAP states and HCP states. The maximum Dice coefficients, reflecting the best spatial matches with HCP states, were significantly higher for real data than for simulated data, $t(18)=7.07$, $p<0.01$. In addition, there was significantly higher variance in Dice coefficients for real data relative to simulated data CAP states, $t(18)=4.99$, $p<0.01$, suggesting better specificity of spatial matches in real data (Fig S5).

Together, results of these simulations support the validity of network states emerging from co-activation pattern analyses in this study.

Reliability of dynamic functioning of CAP states within subject. We previously reported on within-subject reliability of dynamic measures, including time-in-state, in the HCP sample (4). In that normative sample, we observed high reliability in time-in-state and other dynamic measures over consecutive scans (see (4) for discussion).

To evaluate within-subject reliability of network dynamics in the present sample, we calculated the Spearman Brown corrected correlation coefficient for split-half time-in-state (odd and even volumes) for each state and timepoint (rest 1, rest 2) (13). Reliability was high for time-in-state for all states and both timepoints of evaluation, rs>0.93 (Table S6).

Finally, we performed analyses to test whether changes in time-in-state between timepoints (change from rest 1 to rest 2) were significantly larger than split-half differences in time-in-state within timepoints. Because this study tested the hypothesis that network dynamics change over the course of early treatment, it is important to demonstrate that such changes are distinguishable from e.g., measurement error. Results of a paired-samples t-test showed that the

magnitude of time-in-states changes from baseline to week 1 was significantly greater than split-half differences in time-in-states, $t(228)=17.04$, $p<0.01$, Cohen's d=1.13 (Figure S6).

Together, these analyses show adequate reliability of within-subject measurement of time-in-state, and highlight that changes in time-in-state from baseline to week 1 are significantly larger than the variance in resampled (split-half) data. Results support that observed differences over the course of early (placebo or sertraline) treatment are meaningful, but these tests should be replicated in independent samples.

Summary of Data Quality and Reliability. Together, these quality and reliability checks performed within the present sample and across independent samples support reliability and validity of the CAP analytic approach, and the potential for dynamic measures to provide information about individual differences in network activity and the extent to which such network activities change as a function of symptom remission or effective treatment. A next step for this research will be to evaluate in large matched independent samples the replication of spatial organization and dynamic properties of CAP states, and their associations with psychopathology and treatment. Although the control analyses above generally support the reliability of the method and of most network states, it remains unknown if distinctive transient networks or distinctive patterns of dynamic functioning emerge in different psychiatric conditions, at different developmental stages, or as a function of other group or individual difference characteristics. If such differences emerge, it will be important to replicate those effects, along with estimating reliability of network dynamics within a population and within a person over time (4). Future research may address these questions.

Exploratory Models and Control Analyses

At the request of an anonymous reviewer, we performed the following exploratory models.

Site control analyses. We repeated mixed-effects models after covarying site. Results showed that the addition of site covariates did not alter the nature or significance of any effects (changes in *p*s<0.008).

Week 8 outcomes. We performed an exploratory linear model in R to test whether changes in time-in-state predicted differences in depression severity at the final (week 8) timepoint, controlling for baseline symptom severity. Results indicated a non-significant trend in which participants who showed the largest increases in time-in-states 2 and 7, and largest decreases in time-in-states 5 and 6, reported marginally lower depression severity at week 8, B= -1.05, F(1,197)=2.89, *p*=0.09. There were no significant differences in week 8 depression severity as a function of other network state dynamics. Together with analyses reported in the main text, these results imply that early changes in transient network state dynamics are primarily associated with the shape of recovery from depression over time (e.g., more rapid recovery) rather than symptom outcomes at the final timepoint of assessment.

Cross-validation analyses. We performed cross-validation analyses to evaluate, in held-out data, the performance of the mixed-effects model testing early network changes as predictors of treatment response.

In the first cross-validation, we evaluated the performance of the model generalizing to new subjects. First, we randomly selected 80% of subjects (by ID code) as a training dataset. In the training dataset, we fitted the mixed effects model testing changes in network dynamics, linear and non-linear effects of time, and interactions between network changes and time effects,

predicting HAMD scores (controlling for treatment group, baseline network dynamics, age and gender). Second, we predicted the model on the held-out test dataset (remaining 20% of subjects) and calculated RMSE of the predictions as a measure of out-of-sample error. We also estimated in-sample error, by predicting the model on the training dataset and calculating RMSE. We iterated the above steps ten times, selecting new random subsets of subject data (80%/20%) for training and test datasets on each iteration. Average out-of-sample RMSE and average in-sample RMSE were computed (for interpretability we also report on RMSE divided by the HAMD range, as RMSE scales with the dependent variable). Finally, we plotted fitted curves for the predicted model (with 90% confidence interval estimated with model-based parametric bootstrapping), together with curves fitted to the test data (model trained on the test data), for each of the ten iterations of testing (Figure S7).

In the second cross-validation, we evaluated the performance of the model generalizing to new levels of observation within subjects. First, we randomly selected 80% of timepoints (by week number) as a training dataset, and fitted the mixed effects model in the training dataset. Second, we predicted the model on the on the held-out test dataset (remaining 20% of timepoints). Out-of-sample RMSE and in-sample RMSE were calculated, as described above. We iterated the above steps ten times, selecting new random subsets of timepoint data (80%/20%). Average out-of-sample RMSE and in-sample RMSE are reported, and plots were generated displaying fitted curves for the predicted model and fitted curves for a model trained on the test data.

Cross-validation results. For the first cross-validation that evaluated generalizability of the model to new subjects, analyses yielded an average out-of-sample RMSE=5.71 ($RMSE/range_{HAMD}$ =0.17) and an average in-sample RMSE=3.08 ($RMSE/range_{HAMD}$ =0.09). For

the second cross-validation that evaluated generalizability of the model to new levels of time within subjects, analyses yielded an average out-of-sample RMSE=4.56 (RMSE/$range_{HAMD}$ =0.13) and an average in-sample RMSE=2.65 (RMSE/$range_{HAMD}$ =0.08). Together, out-of-sample RMSE was higher than in-sample RMSE both when generalizing to new subjects and to new timepoints. But, in support of model performance, both out-of-sample RMSE and the differences between out-of-sample and in-sample RMSE were low relative to the scale of the dependent variable. There is no universal threshold for RMSE, and caution is warranted when comparing out-of-sample and in-sample estimates given differences in sample sizes for training and test datasets (14,15).

In further support of model performance, estimated effects fitted to each held-out dataset (new subjects, or new levels of time within a subject) were within the 90% confidence interval of predicted effects for every iteration (Figure S7). Together, results of these cross-validation analyses provide initial support that the model generalizes to new data, but these findings should be validated in future studies.

Supplementary References

1. Yeo BTT, Krienen FM, Sepulcre J, Sabuncu MR, Lashkari D, Hollinshead M, et al. The organization of the human cerebral cortex estimated by intrinsic functional connectivity. Journal of Neurophysiology. 2011;106(3):1125–65.

2. Choi EY, Yeo BTT, Buckner RL. The organization of the human striatum estimated by intrinsic functional connectivity. Journal of Neurophysiology. 2012;108(8):2242–63.

3. Kaiser RH, Kang MS, Lew Y, Van Der Feen J, Aguirre B, Clegg R, et al. Abnormal frontoinsular-default network dynamics in adolescent depression and rumination: a preliminary resting-state co-activation pattern analysis. Neuropsychopharmacology. 2019;44(9):1604–12.

4. Janes AC, Peechatka AL, Frederick BB, Kaiser RH. Dynamic functioning of transient resting-state coactivation networks in the Human Connectome Project. Hum Brain Mapp. 2020 Feb 1;41(2):373–87.

5. Murray L, Maurer JM, Peechatka AL, Frederick BB, Kaiser RH, Janes AC. Sex differences in functional network dynamics observed using coactivation pattern analysis. Cognitive Neuroscience. 2021 Mar 18;1–10.

6. Goodman ZT, Bainter SA, Kornfeld S, Chang C, Nomi JS, Uddin LQ. Whole-Brain Functional Dynamics Track Depressive Symptom Severity. Cerebral Cortex. 2021 Oct 1;31(11):4867–76.

7. Yang H, Zhang H, Di X, Wang S, Meng C, Tian L, et al. Reproducible coactivation patterns of functional brain networks reveal the aberrant dynamic state transition in schizophrenia. NeuroImage. 2021 Aug;237:118193.

8. Liu X, Duyn JH. Time-varying functional network information extracted from brief instances of spontaneous brain activity. Proceedings of the National Academy of Sciences of the United States of America. 2013;110(11):4392–7.

9. Warton DI, Hui FKC. The arcsine is asinine: the analysis of proportions in ecology. Ecology. 2011 Jan;92(1):3–10.

10. Cordes D, Haughton VM, Arfanakis K, Carew JD, Turski PA, Moritz CH, et al. Frequencies contributing to functional connectivity in the cerebral cortex in "resting-state" data. American Journal of Neuroradiology. 2001;22(7):1326–33.

11. Whitfield-Gabrieli S, Nieto-Castanon A. Conn: A functional connectivity toolbox for correlated and anticorrelated brain networks. Brain Connectivity. 2012;

12. Rousseeuw PJ. Silhouettes: A graphical aid to the interpretation and validation of cluster analysis. Journal of Computational and Applied Mathematics. 1987;20:53–65.

13. Spearman C. The proof and measurement of association between two things. American Journal of Psychology. 1904;15:72–101.

14. James G, Witten D, Hastie T, Tibshirani R. An Introduction to Statistical Learning [Internet]. New York, NY: Springer New York; 2013 [cited 2022 Feb 25]. (Springer Texts in Statistics; vol. 103). Available from: http://link.springer.com/10.1007/978-1-4614-7138-7

15. Hastie T, Tibshirani R, Friedman J. The Elements of Statistical Learning: Data Mining, Inference, and Prediciton. 2nd ed. Springer; 2017.

Supplementary Tables

Table S1. Neuroimaging parameters

	Columbia University	**Massachusetts General Hospital**	**University of Michigan**	**University of Texas Southwestern Medical Center**
Scanner				
Type	General Electric 3T	Siemens 3T	Phillips 3T	Phillips 3T
Structural Scan				
Series	IR FSPGR	MPRAGE	TFE	MPRAGE
Repetition time/Echo time (TR/TE)	6.0ms/2.4ms	2.3s/2.54ms	8.1ms/3.7ms	8ms/3.7ms
Flip Angle	9º	9º	12º	12º
Thickness	1mm	1mm	1mm	1mm
Resolution	1x1x1mm	1x1x1mm	1x1x1mm	1x1x1mm
Duration	5.00 minutes	4.30 minutes	5.29 minutes	4.24 minutes
Functional Scan				
Repetition time/Echo time (TR/TE)	2000ms/28ms	2000ms/28ms	2000ms/28ms	2000ms/28ms
Flip Angle	90º	90º	90º	90º
Thickness	3.1mm	3.1mm	3.1mm	3.1mm
Resolution	3.2x3.2x3.2mm	3.2x3.2x3.2mm	3.2x3.2x3.2mm	3.2x3.2x3.2mm
Matrix	64x64	64x64	64x64	64x64
Duration	6 minutes	6 minutes	6 minutes	6 minutes

Table S2. Transient network state descriptive statistics.

	State QA		Baseline Time in State (As Proportion of Scan Series)						One-Week Time in State (As Proportion of Scan Series)					
	Mot (mm)	Silht	Min	Max	M	*SD*	Skew	Kurt	Min	Max	M	*SD*	Skew	Kurt
State 1	0.118	0.148	0.028	0.361	0.177	0.060	0.003	0.219	0.006	0.389	0.187	0.058	0.036	0.852
State 2	0.106	0.118	0.017	0.328	0.171	0.066	-0.002	-0.432	0.039	0.333	0.179	0.063	-0.001	-0.487
State 3	0.144	0.128	0.000	0.217	0.086	0.042	0.238	-0.434	0.000	0.211	0.097	0.043	0.091	-0.348
State 4	0.150	0.032	0.000	0.378	0.078	0.088	1.642	1.740	0.000	0.389	0.064	0.074	2.063	4.286
State 5	0.171	0.059	0.000	0.156	0.035	0.029	0.952	0.844	0.000	0.128	0.040	0.028	0.566	-0.266
State 6	0.121	0.130	0.033	0.478	0.220	0.062	0.005	1.241	0.056	0.378	0.220	0.059	-0.156	0.080
State 7	0.117	0.104	0.006	0.383	0.165	0.057	0.009	0.417	0.028	0.328	0.160	0.053	0.018	0.287
State 8	0.122	0.073	0.000	0.361	0.067	0.094	1.665	1.486	0.000	0.344	0.054	0.072	1.873	2.838

Note: Mot. = average motion (in mm) associated with a transient network state. Slht. = average silhouette score for each transient network state, a measure of how cohesive is a cluster of data partitioned together in clustering analysis. Min = minimum, Max = maximum, M = mean, SD = standard deviation, Skew = skewness of the distribution, Kurt = kurtosis of the distribution. Quality assurance checks showed that network states 4 and 8 showed unacceptably high skewness and/or kurtotic distribution. Therefore, time-in-states for these network states were natural log transformed before inclusion in subsequent analyses.

Table S3. Correlations among dynamic measures at baseline, one-week, or changes over time.

Baseline Time in State (As Proportion of Scan Series)								
State	1	2	3	4	5	6	7	8
BASE	*r*	*r*	*r*	*r*	*r*	*r*	*r*	*r*
State 1	1.00	-0.01	**0.68**	-0.60	0.09	0.20	0.01	-0.57
State 2		1.00	-0.21	-0.52	-0.26	0.19	**0.65**	-0.55
State 3			1.00	-0.55	0.62	0.20	-0.15	-0.49
State 4				1.00	-0.39	-0.65	-0.52	**0.95**
State 5					1.00	**0.55**	-0.19	-0.36
State 6						1.00	0.16	-0.67
State 7							1.00	-0.57
State 8								1.00
One-Week Time in State (As Proportion of Scan Series)								
State	1	2	3	4	5	6	7	8
1-WK	*r*	*r*	*r*	*r*	*r*	*r*	*r*	*r*
State 1	1.00	-0.32	**0.67**	-0.46	0.07	0.01	-0.05	-0.46
State 2		1.00	-0.32	-0.39	-0.29	0.09	**0.59**	-0.43
State 3			1.00	-0.50	0.61	0.01	-0.22	-0.44
State 4				1.00	-0.34	-0.56	-0.47	**0.93**
State 5					1.00	**0.42**	-0.35	-0.29
State 6						1.00	0.07	-0.54
State 7							1.00	-0.53
State 8								1.00
Change from Baseline to One-Week Time in State (As Proportion of Scan Series)								
State	1	2	3	4	5	6	7	8
CHNG	*r*	*r*	*r*	*r*	*r*	*r*	*r*	*r*
State 1	1.00	-0.39	**0.54**	-0.30	-0.22	-0.13	-0.28	-0.36
State 2		1.00	-0.37	-0.03	-0.35	-0.34	**0.31**	-0.09
State 3			1.00	-0.42	0.38	-0.13	-0.35	-0.35
State 4				1.00	-0.36	-0.40	-0.05	**0.65**
State 5					1.00	**0.54**	-0.32	-0.26
State 6						1.00	-0.31	-0.28
State 7							1.00	-0.16
State 8								1.00

Note: Reported are Pearson's correlation coefficients (*r*) for time-in-state at baseline, time-in-state at one week after initiating treatment, or changes in time-in-state from baseline to one-week. Network states for which dynamic measures were consistently highly correlated are indicated by bolded and shaded cells.

Table S4. Transient network state dynamics descriptive statistics by antidepressant group.

	Sertraline						**Placebo**						**Overall**	
	Baseline (*n*=128)		**One-Week (*n*=110)**		**Change (*n*=110)**		**Baseline (*n*=131)**		**One-Week (*n*=119)**		**Change (*n*=119)**		**Change (*n*=229)**	
	Mean	SD	Mean	SD	Mean	SD	Mean	SD	Mean	SD	Mean	SD	Mean	SD
State 1	0.176	0.059	0.188	0.052	**0.010**	**0.067**	0.179	0.062	0.186	0.064	0.005	0.058	**0.008**	**0.062**
State 2*	0.166	0.061	0.181	0.059	**0.016**	**0.059**	0.176	0.070	0.178	0.068	0.003	0.063	**0.009**	**0.061**
State 3	0.086	0.040	0.100	0.046	**0.013**	**0.042**	0.087	0.044	0.094	0.041	**0.008**	**0.038**	**0.010**	**0.040**
State 4	0.077	0.087	0.060	0.071	**-0.017**	**0.049**	0.077	0.089	0.066	0.075	**-0.014**	**0.044**	**-0.016**	**0.046**
State 5	0.038	0.031	0.043	0.027	0.005	0.033	0.032	0.027	0.038	0.029	**0.008**	**0.026**	**0.006**	**0.029**
State 6*	0.225	0.066	0.216	0.063	-0.007	0.067	0.217	0.058	0.224	0.053	**0.012**	**0.060**	0.003	0.064
State 7	0.165	0.061	0.163	0.053	0.002	0.055	0.164	0.054	0.158	0.053	-0.006	0.048	-0.004	0.051
State 8	0.066	0.094	0.049	0.072	**-0.018**	**0.046**	0.067	0.093	0.055	0.071	**-0.014**	**0.045**	**-0.016**	**0.045**

Note: SD = standard deviation. Bolded and shaded cells represent significant change in time-in-state from baseline to one week after initiating treatment, within each treatment group or across the sample (within-subject t-tests, $p<0.05$). Asterisked state labels represent networks for which the change in time-in-state was significantly different between treatment groups (between-subjects t-tests, $p<0.05$). These tests are post-hoc and intended to expand upon main hypothesis-testing models.

Table S5. Spatial reliability of CAP states across independent samples.

	Dice Coefficients Across Independent Samples							
	EMBARC							
HCP	State 1	State 2	State 3	State 4	State 5	State 6	State 7	State 8
	DSC	*DSC*	*DSC*	*DSC*	*DSC*	*DSC*	*DSC*	*DSC*
State 1	**0.81**	**0.77**	0.22	0.41	**0.71**	0.28	0.27	0.61
State 2	0.58	0.58	0.24	0.29	0.45	0.40	0.33	0.63
State 3	0.74	**0.86**	0.22	0.46	0.63	0.29	0.10	0.51
State 4	0.25	0.17	**0.72**	0.49	0.33	0.70	**0.80**	0.47
State 5	0.62	0.43	0.35	0.26	0.60	0.41	0.57	**0.72**
State 6	0.20	0.28	**0.79**	0.69	0.33	**0.72**	0.67	0.31
State 7	0.37	0.42	0.69	0.58	0.47	0.58	0.58	0.41
State 8	0.35	0.25	0.59	0.42	0.43	0.61	**0.73**	0.52

Note: Reported are Dice similarity coefficients (*DSC*) for spatial organization of network states independently derived in the present sample (EMBARC) and a sample drawn from the Human Connectome Project (HCP; see (4)). DSC values approaching 1.0 indicate high spatial overlap. To indicate potentially "matching" states across samples, DSC values >0.70 are bolded and shaded, with values >0.80 in darker shading.

Table S6. Within-subject split-half reliability of transient network dynamics.

	Split-Half Reliability of Time-in-State	
	Baseline	**One-Week**
	SB *r*	SB *r*
State 1	0.93	0.93
State 2	0.95	0.94
State 3	0.95	0.95
State 4	0.99	0.99
State 5	0.97	0.95
State 6	0.93	0.93
State 7	0.93	0.94
State 8	0.99	0.99

Note: Reported are reliability statistics computed as Spearman Brown corrected correlation coefficients (SB *r*) for split-half time-in-state for each state and timepoint (12).

Supplementary Figures

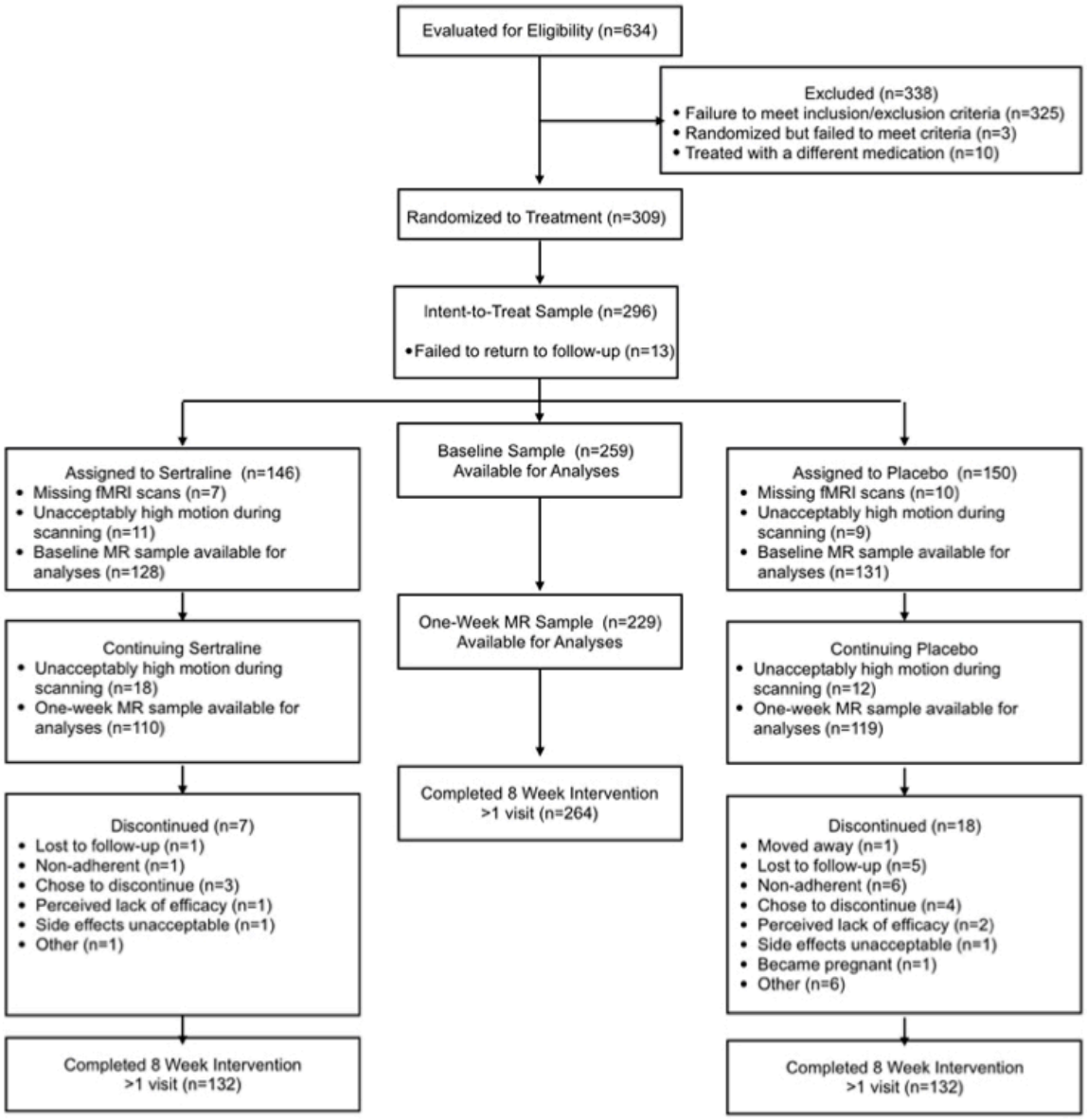

Figure S1. ***Consort diagram***.

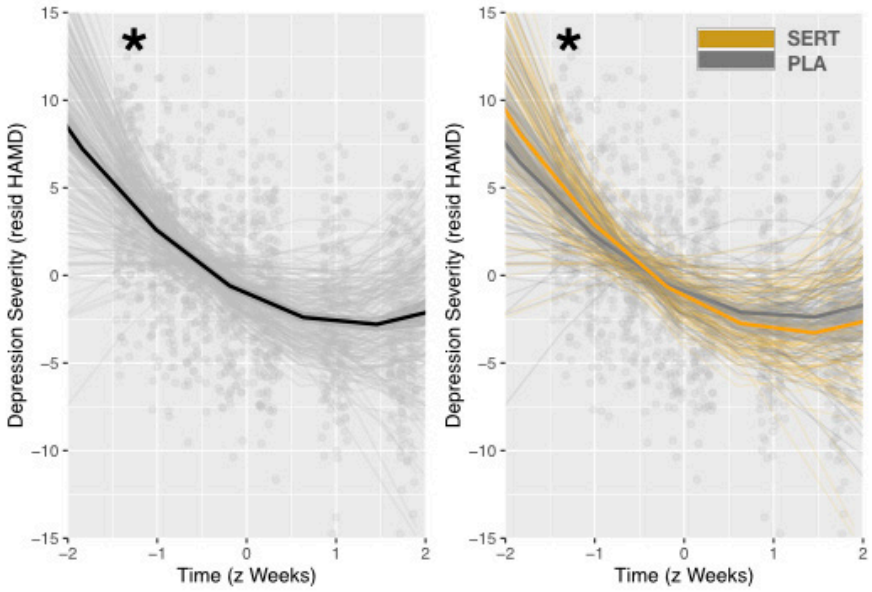

Figure S2. ***Depression recovery over time and as moderated by antidepressant treatment group.*** Patients showed linear and quadratic patterns of symptom change over the eight-week period of treatment, including linear improvement in depression symptom severity that was steepest in early weeks of treatment. Patients in the sertraline group (SERT) showed a steeper linear improvement in depression severity relative to patients in the placebo group (PLA). *Note:* Displayed are scatterplots showing Hamilton Depression scores for patients at all timepoints, and curvilinear within-subject changes in depression severity. Group-level fit lines show symptom change across the full sample (left), or symptom change within the sertraline or placebo groups. Hamilton Depression scores (resid HAMD) are residualized for covariates (age and gender). Time in weeks z-scored, weeks 0 to 8. *$p<0.05$, effects of time, moderating effect of antidepressant treatment.

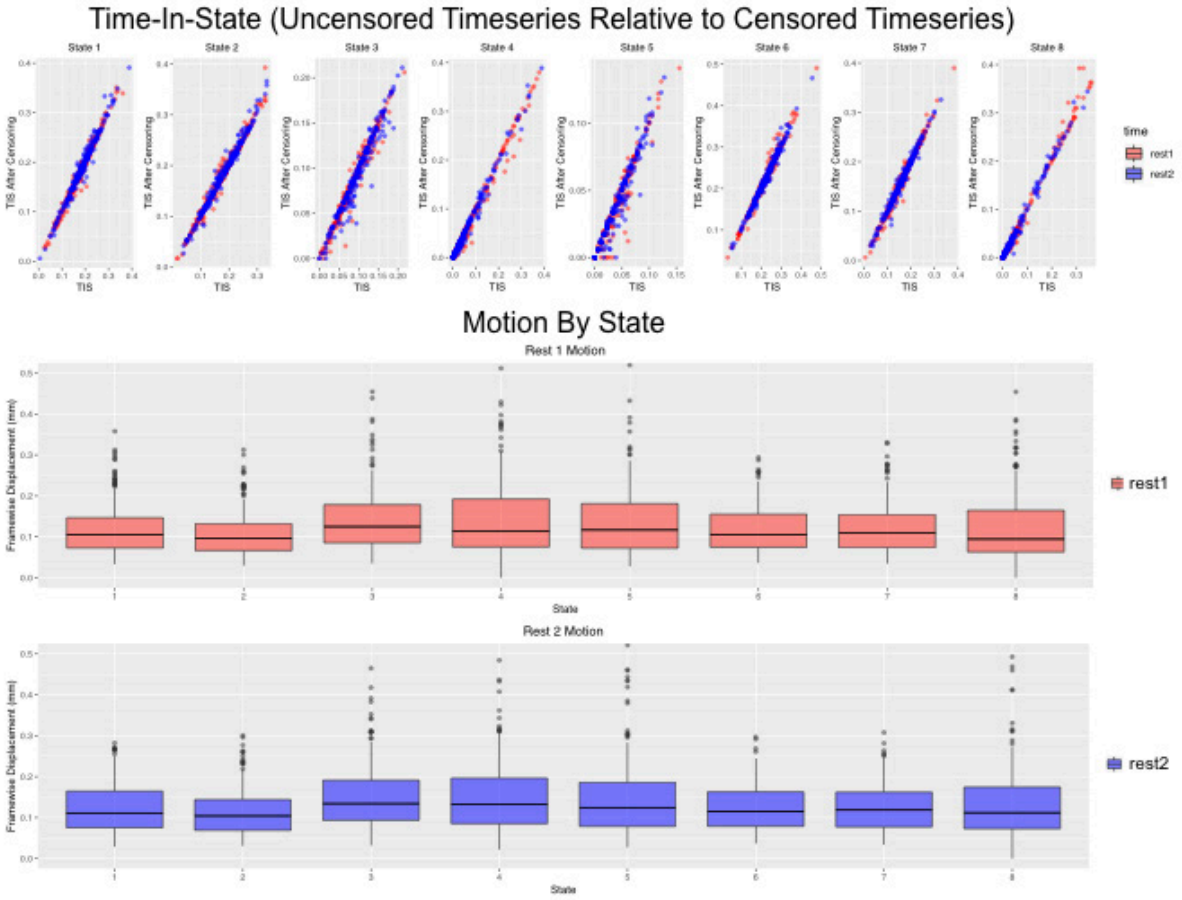

Figure S3. ***Motion checks.*** To ensure that head motion did not influence estimated time-in-states, we censored the timeseries for each participant at a threshold of framewise displacement >0.3mm. Proportional time-in-states of the censored relative to uncensored timeseries were highly correlated (upper panel, r=0.97 to r=0.99). There were no significant changes in time-in-states for any CAP state after censoring (ps>0.05). In addition, there were no differences between transient network states in framewise displacement associated with each state (lower panels; horizontal line indicates median framewise displacement for that state).

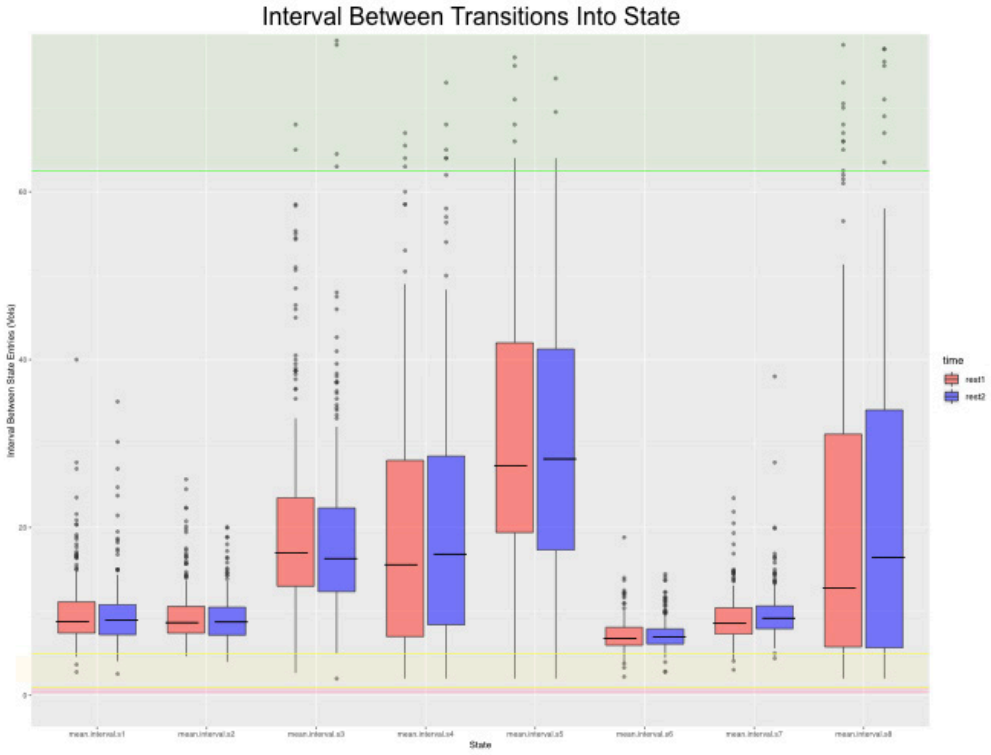

Figure S4. ***Interval between state recurrences.*** Average intervals (number of volumes) between state recurrences (transition into that state, after time spent in any other state) are displayed. The mean intervals between state recurrences ranged from 7.17 to 33.54 volumes (14.43 to 67.08 seconds per cycle, or 0.015 to 0.070 Hz). Recurrence frequencies for all states fell within the standard band-pass filter for resting-state functional connectivity analyses, of 0.008 to 0.090 Hz (11). Typical noise frequency bands are displayed for respiration, 0.1-0.5 Hz (yellow), cardiac activity, 0.6-1.2 Hz (pink), and scanner drift, <0.008 Hz (green) (10). Horizontal lines within boxplot indicate median interval between state recurrences for each state and timepoint.

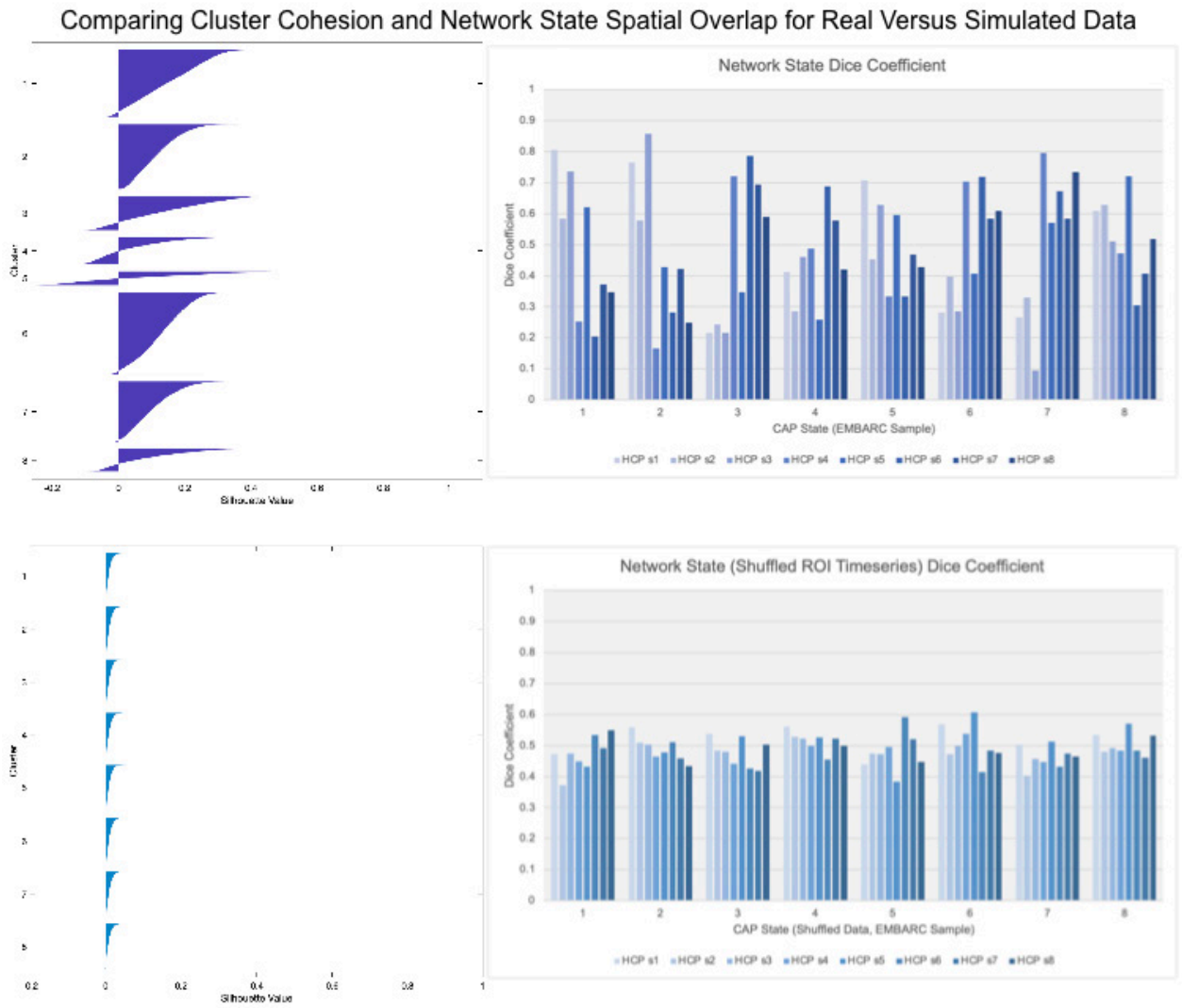

Figure S5. ***Comparing co-activation pattern (CAP) network states derived from real versus simulated (shuffled) data.*** Simulated data were created from the real dataset by shuffling the timeseries of activation of each ROI with respect to other ROIs but maintaining the integrity of the timeseries within each ROI, and then performing the same CAP analysis on simulated data. The top panel shows silhouette scores and Dice coefficients for the eight CAP states presented in this study; the bottom panel shows silhouette scores and Dice coefficients derived from simulated data. (Dice coefficients indicate spatial overlap between network states and independent states derived in the Human Connectome Project data using the same analytic approach (4)). Comparing silhouette scores between real and simulated data, silhouette scores were significantly higher for real data CAP states than for simulated data CAP states, $t(228)=62.30$, $p<0.01$. The maximum Dice coefficients, reflecting the best spatial matches with HCP states, were significantly higher for real data than for simulated data, $t(18)=7.07$, $p<0.01$, and there was significantly higher variance in Dice coefficients for real data relative to simulated data CAP states, $t(18)=4.99$, $p<0.01$, suggesting better specificity of spatial matches in real data.

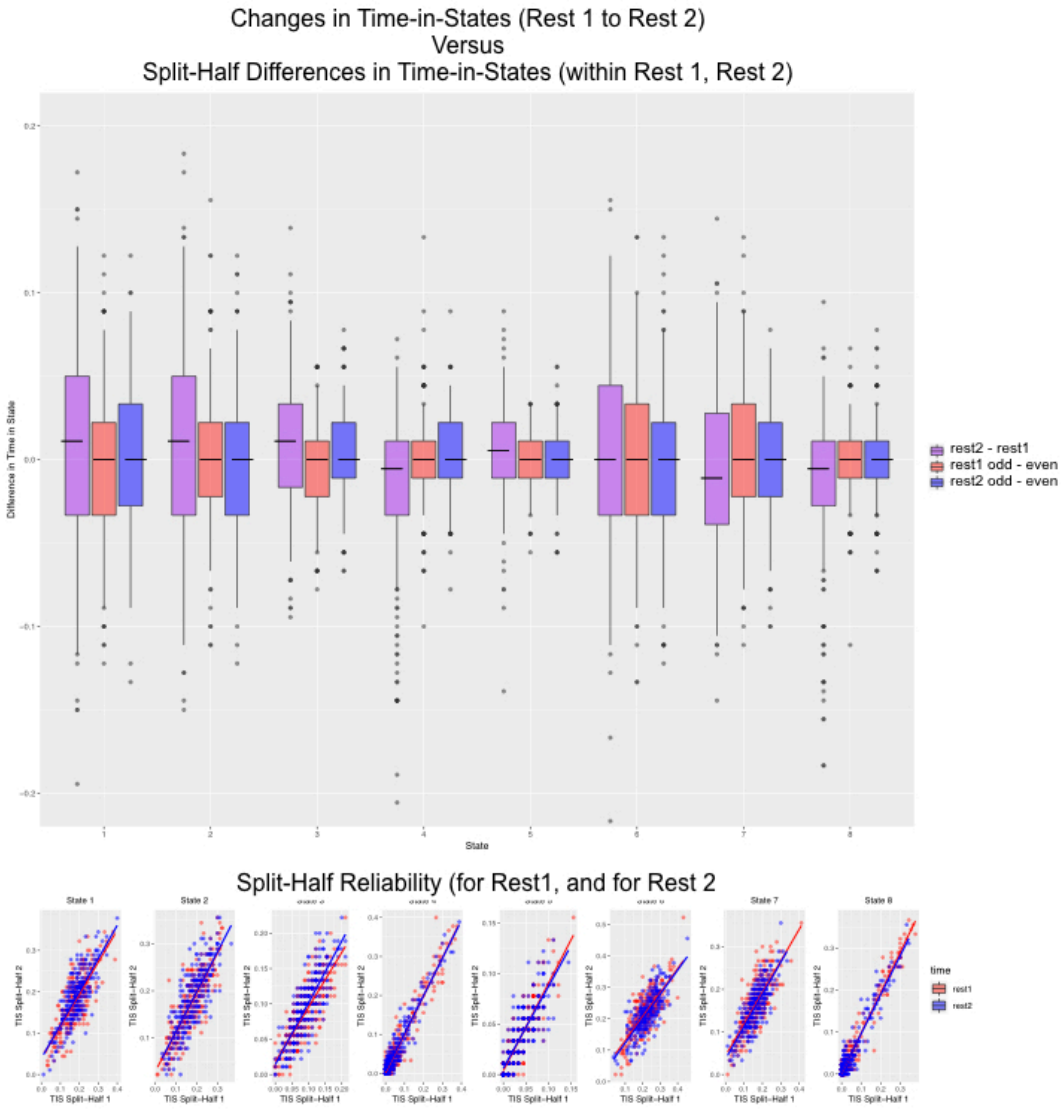

Figure S6. ***Comparing within-subject changes in network dynamics: Changes over time versus reliability of measures.*** Upper panel shows average within-subject change in time-in-state from baseline to week 1 of treatment for each network state (purple; rest2-rest1), together with average within-subject differences in time-in-state between split-halves at either baseline (red; rest1, odd-even volumes) or week 1 (blue; rest2, odd-even volumes). To support the validity of the measure and interpretation of effects, magnitude and range of changes over early treatment should exceed magnitude of differences within a timepoint. Indeed, magnitude of time-in-states changes from baseline to week 1 was significantly greater than split-half differences in time-in-states, $t(228)=17.04$, $p<0.01$, Cohen's $d=1.13$. Lower panel shows the correlation in time-in-states between split halves at each timepoint, and Spearman Brown corrected correlation coefficients indicated high reliability for all states and both timepoints (Table S6).

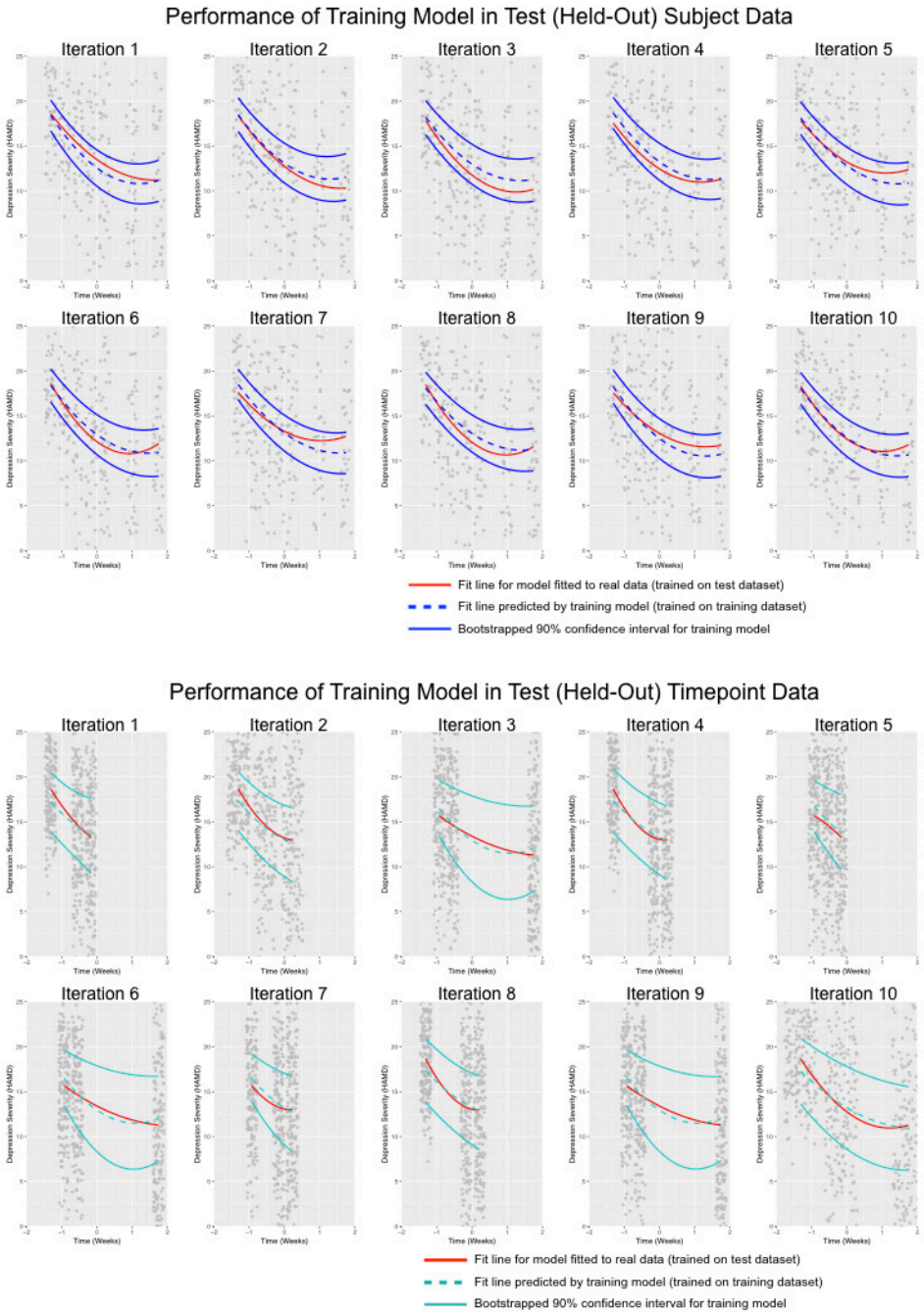

Figure S7. ***Model performance.*** Cross-validation analyses evaluated the performance of the mixed-effects model that tested early network changes as predictors of treatment response. The first cross-validation tested generalizability of the model to new subjects (upper panels) and the second tested generalizability of the model to new levels of observation within subjects (lower panels). In each of ten iterations of analysis for each cross-validation, we randomly selected 80% of the data (80% of subjects, or 80% of timepoints) as a training dataset and fitted the mixed effects model, then predicted the model on the held-out test dataset (remaining 20% of subjects or timepoints). Displayed are fitted curves for the predicted model (blue or cyan dashed lines) with 90% confidence interval estimated with model-based parametric bootstrapping (blue or cyan solid lines), together with fitted curves for a model trained on the test data (red lines).